EPA-600/2-76-277
November 1976

Environmental Protection Technology Series

REMOTE MONITORING OF NITRIC OXIDE BY GAS-FILTER CORRELATION TECHNIQUES

Environmental Sciences Research Laboratory
Office of Research and Development
U.S. Environmental Protection Agency
Research Triangle Park, North Carolina 27711

RESEARCH REPORTING SERIES

Research reports of the Office of Research and Development, U.S. Environmental Protection Agency, have been grouped into five series. These five broad categories were established to facilitate further development and application of environmental technology. Elimination of traditional grouping was consciously planned to foster technology transfer and a maximum interface in related fields. The five series are:

1. Environmental Health Effects Research
2. Environmental Protection Technology
3. Ecological Research
4. Environmental Monitoring
5. Socioeconomic Environmental Studies

This report has been assigned to the ENVIRONMENTAL PROTECTION TECHNOLOGY series. This series describes research performed to develop and demonstrate instrumentation, equipment, and methodology to repair or prevent environmental degradation from point and non-point sources of pollution. This work provides the new or improved technology required for the control and treatment of pollution sources to meet environmental quality standards.

This document is available to the public through the National Technical Information Service, Springfield, Virginia 22161.

EPA-600/2-76-277
November 1967

REMOTE MONITORING OF NITRIC OXIDE BY GAS-FILTER CORRELATION TECHNIQUES

by

Darrell E. Burch and David A. Gryvnak

Ford Aerospace & Communications
Corporation Formerly Known As

Aeronutronic Ford Corporation
Aeronutronic Division
Newport Beach, California 92663

Contract No.

68-02-0766

Project Officer

William F. Herget
Emission Measurement and Characterization Division
Environmental Sciences Research Laboratory
Research Triangle Park, North Carolina 27711

ENVIRONMENTAL SCIENCES RESEARCH LABORATORY
OFFICE OF RESEARCH AND DEVELOPMENT
U.S. ENVIRONMENTAL PROTECTION AGENCY
RESEARCH TRIANGLE PARK, NORTH CAROLINA 27711

DISCLAIMER

This report has been reviewed by the Environmental Sciences Research Laboratory, U.S. Environmental Protection Agency, and approved for publication. Approval does not signify that the contents necessarily reflect the views and policies of the U.S. Environmental Protection Agency, nor does mention of trade names or commercial products constitute endorsement or recommendation for use.

ABSTRACT

The feasibility of remotely monitoring the concentration of Nitric Oxide (NO) in the effluent of industrial stacks has been investigated analytically and experimentally in the laboratory. The type of instrument considered employs two or more gas-filter cells that contain different amounts of NO. Radiant energy emitted by the hot gas in the effluent is measured after it has passed either through one of the gas-filter cells or through a neutral density filter. By comparing the amounts of energy received through each of the filters, it is possible to determine the concentration of NO in the presence of a moderate amount of continuum-emitting material such as small particles. A simple, single-line spectral model served as the basis for the analytical work. Heated cells containing NO + N_2 or H_2O + N_2 simulated an industrial stack for the laboratory experiments. Interference by hot H_2O in the effluent and cold H_2O in the atmospheric path causes the most serious uncertainties in the measurements for many types of stacks.

CONTENTS

		Page
Abstract		iii
Figures		vi
Abbreviations		viii
I	Introduction	1
II	Summary	3
III	Conclusions	5
IV	Recommendations	7
V	Illustration of the Spectroscopic Principles of Remote Sensing by use of a Simple Analytical Model	9
VI	Experimental Procedures	36
VII	Results of Laboratory Measurements	52
References		69

FIGURES

Number		Page
1	Optical Schematic Diagram of an Instrument of the Type on Which the Calculations of Section V are based.	10
2	Plot of Transmittances of GFC and Neutral-Density Filter Combinations.	12
3	Plots of $N_\nu^B \epsilon_s T_{att}$ vs $(\nu - \nu_o)$ for Two Samples with ϵ_s in the Non-Linear Region Near the Line Center	14
4	Plots of $N_\nu^B \epsilon_s T_{att}$ vs $(\nu - \nu_o)$ for Two Samples with ϵ_s Near the Linear Region.	16
5	Spectral Plots of $N_\nu^B \epsilon_s T_j$ vs $(\nu - \nu_o)$ for the Attenuator and Two GFC's.	18
6	Spectral Plots of $N_\nu^B \epsilon_s T_{0.1}$ vs $(\nu - \nu_o)$ for Two Temperatures. .	19
7	Spectral Plots of $N_\nu^B \epsilon_s T_1$ vs $(\nu - \nu_o)$ for Two Temperatures. . .	20
8	Semi-Logarithmic Plots of Y_j vs w for Various Samples	21
9	Plots of Z_j vs u for Various GFC's	23
10	Plots of Z_j vs Temperature for Various GFC's	24
11	Semi-Logarithmic Plots of Y_j vs w for Two Small Samples at Different Temperatures with the Same Value of Y_{att}	26
12	Spectral Plots of $N_\nu^B \epsilon_s T_{att}$ for Three Samples at 450 K.	27
13	Plots of Z_1 vs u for Five Different Values of ϵ_c	29
14	Plots of $Z_{0.1}$ vs u for Five Different Values of ϵ_c	30
15	Plots of ϵ_c vs u for Five Different Values of Z_1	31
16	Plots of ϵ_c vs u for Three Different Values of $Z_{0.1}$.	32
17	Plots of θ_s vs u for Five Different Values of ϵ_c	33

FIGURES (CONTINUED)

Number		Page
18	Optical Diagram of the Apparatus Used With a 1.42-cm Sample Cell .	37
19	Optical Diagram of the Apparatus Used With a 200-cm Sample Cell. .	41
20	Transmission Spectra of H_2O and NO and of the Bandpass of the Grating Assembly	43
21	Logarithmic Plots of the Average Absorptance of NO + N_2 Mixtures vs u for Two Temperatures.	53
22	Logarithmic Plots of Y_j vs u for NO + N_2 Mixtures at 450 K	55
23	Semi-Logarithmic Plots of Z_j vs u for Four Sample Temperatures . .	57
24	Logarithmic Plots of Y_j vs u for Samples of NO + N_2 with Additional Continuum Emission.	60
25	Semi-Logarithmic Plots of Z_j vs u for Samples of NO + N_2 with Additional Continuum Emission.	61

ABBREVIATIONS AND SYMBOLS

x --species of gas being measured

GFC --gas-filter cell that contains gas of species x

C --concentration of gas species x (ppm)

p --partial pressure of a gas species (atm)

P --total pressure of a gas mixture (atm)

ℓ --length of optical path through a gas

θ --temperature of gas (K). A subscript s denotes the temperature of the sample

u --absorber thickness of gas of species x in the sample (atm cm or ppm meters). $u = p\ell$. 1 atm cm $= 10^4$ ppm meters

w --absorber thickness of gas of species x in a gas-filter cell at 300 K (atm cm). $w = p\ell$.

ν, ν_o --wavenumber (cm^{-1}). ν_o denotes the center of an absorption line

T --transmittance that would be observed with infinite resolving power. Subscripts denote different gases or optical components as follows: s, sample that may include gas species x as well as other gas species. s,x gas species x in sample. s,y gas species other than x in sample. s,c continuum in sample.

--The index letter j denotes a GFC. A specific GFC may be identified by a letter b, c, etc., or by a number such as 1.0, or 0.1 that indicates the value of w for that particular GFC. For example, T_b is the transmittance of GFC-b, (gas-filter cell b) including its associated neutral density filter. $T_{b,g}$ and $T_{b,n}$ represent the transmittances of the gas only, and the neutral-density filter only, respectively, of GFC-b. $T_b = T_{b,n}\, T_{b,g}$. T_{att}, transmittance of the attenuator not associated with a particular GFC. T_{fil}, denotes the transmittance of the filter, or combination of filters, that determines the spectral bandpass.

$\overline{T}$ --average transmittance over the spectral interval of interest

A --absorptance (1-T)

ϵ --emissivity. The subscripts used with T also apply for $\overline{T}$, A, $\overline{A}$, ϵ, and $\overline{\epsilon}$

N_ν^B --spectral radiance of a blackbody at the temperature of the hot sample [μwatts/(cm^2 cm^{-1} ster)]

k --absorption coefficient due to a single line of gas species x.

$$k = \frac{S}{\pi} \frac{\alpha}{(\nu - \nu_o)^2 + \alpha^2} = \frac{-\ell n\, T}{u}$$

S --$\int k d\nu$, strength of the absorption line (atm cm)$^{-1}$ cm^{-1}

α --half-width of absorption line (cm^{-1}). $\alpha = \alpha^o p\, (300/\theta)^{1/2}$

E --radiant power incident on the detector from the sample. A subscript denotes the GFC through which the radiant energy passes.

Y_j --$\int N_\nu^B \epsilon_s T_j \, d\nu$, a quantity proportional to the radiant power (μwatts cm^{-2} $ster^{-1}$) reaching the detector from the sample through a GFC indicated by the subscript index j. Substitution of a, b or 0.1, etc. for j denotes a specific GFC; substitution of att for j denotes the attenuator that is not associated with a particular GFC (see Equation (7)).

M --E_j/Y_j. A factor that accounts for losses, for the length of the optical path between the emitting gas and the detector, and for the sizes of the detector and the collecting optics (see Equation (7)).

D_j --detector signal resulting from the chopped energy beam

R_j --responsivity of the detector. $R = D_j/\Delta E_j$, where ΔE_j is the difference between the radiant power levels on the detector during the two halves of the chopper cycle.

Z_j --$(Y_{att} - Y_j)/Y_{att}$ (see Equation (8)).

SECTION I

INTRODUCTION

Full-time monitoring of all potentially polluting industrial stacks is obviously a costly task that would require thousands of instruments. Many stacks operate most of the time with the amount of polluting gas in the effluent well within EPA or local standards. Therefore, continuous monitoring of all of these stacks would be quite inefficient. For many inspection purposes, it would be adequate to spot check these stacks periodically to see that they meet standards. An attractive approach to spot-inspection involves a remote, passive monitor that could operate from a road-side or from a parking lot at distances as large as 200-300 m from a stack. Such an instrument could be operated at any time of day by inspectors with no cooperation required on the part of the management of the plant in which the stack is located. The work reported here has dealt mostly with the remote monitoring of NO, one of the major pollutant gases in the effluent from stationary sources.

A class of instruments that employ gas-filter cells (GFC's) as the key component have demonstrated good performance as monitors of several gases, including NO, that exhibit sharp structure in their infrared spectra. In these instruments the sample gas absorbs energy emitted by a radiant energy source that is a part of the instrument. The GFC contains the gas species that is to be monitored in a sample that may contain several other gas species and particulate matter. The good sensitivity and good discrimination possible with these relatively simple instruments result from the correlation between the spectral structure of the gas in the GFC and that of the gas species to be measured in the sample. Strong positive correlation exists if there is sharp structure in the spectra because both gases are the same species. Without the need for complicated, inefficient dispersing instruments, the GFC provides a simple means of comparing spectral structures with very high effective resolution; the spectral resolution corresponds approximately to the widths of the separate spectral intervals that are opaque near each absorption line of the gas in the GFC. Most instruments employing GFC's do not require the beam to be well collimated nor to be passed through a narrow slit; consequently, the "throughput" of radiant energy can be quite high.

The purpose of the analytical and laboratory work reported here has been to investigate the feasibility of extending gas-filter correlation techniques to passive, remote sensing of pollutant gases in the effluent from industrial stacks. Although many of the principles and findings apply to any gas species, the emphasis has been on NO. Field instruments of the type studied receive infrared radiant energy emitted by the hot gas being investigated. The concentration of NO is to be determined by measuring the different amounts of infrared

energy received from the hot gas through a series of filters. Two or more of the filters contain NO, or whatever other gas species is being measured. Another filter may simply be a neutral-density attenuator. At least in principle, the measurements through the attenuator and two or more GFC's provide enough information that the NO concentration in the stack effluent can be determined without knowing the gas temperature or the amount of continuum energy emitted by particulate matter that may also be in the effluent.

Under a previous contract with with EPA,[1] we designed and built an across-the-stack instrument to measure the concentration of either NO, CO, SO_2, HCl or HF in the effluent from stationary emission sources. Although the sample gas is studied in absorption in this previously built instrument, many of the principles are the same as in a passive instrument. Thus, many of the findings of the previous work have been carried over to the present investigation. The most important part of the design of the NO channel of the across-the-stack instrument was not in obtaining sensitivity but in minimizing interference by H_2O vapor. The hot H_2O vapor is present in most stack effluent and has several absorption lines in the only infrared region where NO absorbs or emits significantly. The research performed as part of the previous contract led to the conclusion that the least interference by H_2O vapor was realized if the instrument operated in the spectral band from approximately 1896 cm^{-1} to 1907 cm^{-1}. Most of the laboratory tests of the present contract were performed with the instrument adjusted to this 11-cm^{-1} wide spectral interval.

---

1. Burch, D. E. and D. A. Gryvnak. Infrared Gas Filter Correlation Instrument for In-Situ Measurement of Gaseous Pollutants. EPA-650/2-74-094, Environmental Protection Agency, Washington, D.C. Prepared by Aeronutronic Ford Corp., under Contract No. 68-02-0575, December 1974. Also, Burch, D. E. and D. A. Gryvnak, "Cross-Stack Measurement of Pollutant Concentrations Using Gas-Cell Correlation Spectroscopy," Chapter 10 of Analytical Methods Applied to Air Pollution Measurements, R. K. Stevens and W. F. Herget (Eds.) Ann Arbor Science Publishers, Ann Arbor, Michigan, 1974, pp 193-231.

SECTION II

SUMMARY

The optical principles and the problems involved in the passive, remote sensing of NO in the effluent from stationary sources have been investigated analytically and experimentally. The type of instrument considered employs gas-cell correlation techniques with one or more gas-filter cells that contain different amounts of NO. Each GFC acts as a highly selective filter that absorbs strongly near the center of each NO absorption line. The widths of the spectral intervals of strong absorption are different for each GFC because of the different amounts of NO.

The hot NO in the effluent gas under study also emits strongly, according to Kirchoff's law, at the same wavenumbers where the GFC's absorb strongly. The instrument compares the relative amounts of energy emitted by the hot NO that are transmitted through each of the GFC's as well as through an attenuator that has constant transmittance over the spectral interval passed. From the comparison, it is possible to obtain information that is related to the spectral shape of the NO emission near each line. From this information, it is possible to determine the product $C\ell$ of the NO in the hot gas without knowing the gas temperature or the amount of emitted energy that is due to continuum emission from particles or other gases. C is the concentration, and ℓ is the optical path length through the sample.

The analytical part of the investigation is discussed in Section V and is based on a simple spectral model that consists of a single spectral line. The strength and width parameters assigned to the model line are similar to those of a typical NO line in the spectral interval being considered for a field instrument. A simple computer program has been used to make very precise calculations of the emitted and absorbed energy based on the one-line model. It is assumed that energy emitted by the hot gas is transmitted through either one of the GFC's or the attenuator to a detector. The spectral radiance of the hot gas and the transmitted power are calculated for a very narrow spectral interval over which the spectral radiance is nearly constant. Each such calculation is repeated for adjacent narrow intervals; the results for all intervals are then summed to integrate over the spectral interval from the center of the single model line to a point midway to where the next line center would be. The calculations have been repeated for a variety of hot sample temperatures and gas concentrations and with different amounts of continuum emission contained in the hot sample.

Several figures illustrate the spectroscopic principles of detection and the effects of changing the different parameters: the amount of emitting gas, sample temperature, continuum emissivity, and amount of gas in a GFC. Three separate

measurements of the apparent spectral radiance of a hot sample as observed separately through an attenuator and two properly selected GFC's are sufficient for the determination of the gas concentration without a-priori knowledge of the gas temperature or of the amount of continuum emission.

Section VI describes the laboratory apparatus and procedures used to make a series of measurements under simulated field conditions. Either one of two heated cells contained samples of NO + N_2 or of H_2O + N_2 to simulate the effluent from a stack. The shorter, 1.42-cm, cell was employed for several mixtures of different NO concentrations between 1% and 100% with sample temperatures between approximately 410 K and 450 K. A sapphire disk was placed next to the hot sample cell for a few of the measurements to investigate the effect of continuum emission in addition to the emission by NO. The continuum emission simulated emission by particulate matter in typical stack effluent.

A double-pass cell with a 200-cm optical path-length was heated to 445 K to contain samples of H_2O + N_2. Transmission spectra of the hot H_2O were obtained, and the interference caused by emission from this hot gas was investigated. Even in the optimum spectral interval for NO monitoring, the hot NO in a typical stack of interest probably emits less infrared energy than the hot H_2O. Thus, the monitoring instrument must discriminate well against H_2O to avoid having this gas produce serious errors.

A small grating assembly that resembles a grating monochromator served as a narrow bandpass filter. Most of the measurements were made with the grating assembly adjusted to pass the 1896 - 1907 cm^{-1} interval, which was selected because the H_2O absorption is less than in any other interval of similar width in the strong part of the NO band. A few data on H_2O interference were also obtained with the spectral interval shifted a few cm^{-1} in each direction.

Two GFC's, each 1 cm long, were employed in the laboratory apparatus; one contained 1 atm of NO, and the other, 0.1 atm. The two GFC's and an attenuator were mounted on a sliding assembly that allowed either of the three components to be moved easily into the beam of energy emitted by the hot sample under study. The energy beam was chopped at 450 Hz and was detected by an InSb detector cooled by liquid nitrogen. The detector signal was processed by a synchronous demodulator and amplifier to produce a dc voltage proportional to the chopped energy on the detector. Three separate signal measurements were made for each sample, one with each GFC and one with the attenuator in the beam. Convenient parameters based on the relative values of the three signals were related to sample conditions. The results have been presented in graphical and tabular form. These results provide most of the information on the spectral properties of hot NO and on the characteristics of the GFC's containing NO that is required to estimate the sensitivity of a field instrument of the type considered here. The data on H_2O interference also make it possible to estimate the performance limitations imposed by this gas.

SECTION III

CONCLUSIONS

Gas-filter correlation techniques have been shown to be quite adaptable to the remote sensing of NO because of the sharp spectral structure due to the strong, well-separated absorption lines of this gas. In addition, the strong vibration-rotation lines of NO occur in the spectral region (near 1900 cm^{-1}) for which there are sensitive detectors and where the spectral radiance is relatively high for a blackbody near the temperature of stack effluent.

The number and types of radiometric measurements required to determine the NO concentration in a sample plume depend on the nature of the source of emitted energy and on the amount of information that can be determined by other methods. In all cases, we assume: that the NO concentration and the temperature are uniform over the optical path through the plume; that the length of the optical path through the plume can be determined by other methods; the plume is at 1 atm pressure; the temperature and amount of the emitting NO are high enough that the emitted power can be measured without serious errors due to detector noise; emission by the chopper and other instrument components can be accounted for; interference by clouds and the atmosphere beyond the plume can be accounted for; the instrument is sensitive only to energy in one selected spectral interval; and the instrument has been calibrated so that detector signals can be related directly to the amount of radiant power on the detector.

In the simplest case, the sample plume temperature is known and the plume contains no material, other than NO, that emits infrared energy in the spectral interval of interest. In this case, the concentration of NO can be determined from a single radiometric measurement without a gas-filter cell. In a less-simple case, the temperature is known, but other gases and/or particulate matter in the plume emits an unknown amount of continuum energy; we assume that the emissivity ϵ_c of the continuum is the same for all wavenumbers. Two radiometric measurements are then required to determine the concentration of NO in such a plume. One radiometric measurement is made directly, or with the energy passing through a neutral-density attenuator; the other is made through a properly chosen GFC filled with NO. If the temperature is unknown and there is continuum emission, three radiometric measurements are required: one directly or through a neutral-density attenuator, and one each through two separate GFC's that contain different amounts of NO.

Interference by H_2O probably imposes the most serious limitation on the performance of a remote NO monitor of the type considered here. Absorption by H_2O in the atmospheric path between the plume and the instrument causes some unavoidable interference; this interference can probably be accounted for reasonably

well for most field conditions. The most serious interference results from the emission by H_2O in the hot plume being monitored. The spectrum of the energy emitted by the H_2O contains spectral structure that makes it impossible to treat the H_2O emission as continuum emission. In order to accurately account for the H_2O emission, it is necessary to determine ahead of time the response of the instrument to emission by a variety of H_2O samples at different temperatures. The H_2O concentration in the plume must then be estimated by other methods so that the radiometric measurements can be adjusted to account for the H_2O interference.

The spectral interval between 1896 and 1907 cm^{-1} is probably about the best compromise based on the amount of radiant energy emitted by NO and on the minimum interference by H_2O. Wider spectral intervals would increase the amount of energy received, making it possible to use detectors of lower detectivity and/or smaller collecting optics. However, the interference by H_2O increases rapidly as the interval is widened or shifted. Use of a spectral interval significantly narrower than the recommended 11-cm^{-1} wide one would decrease the amount of the radiant power received to the point that detector noise might become a limiting factor in the measurement accuracy. In addition, interference filters for this spectral region ($\approx$ 1900 cm^{-1}) with a bandpass narrower than approximately 11 cm^{-1} are much more difficult to fabricate than ones with a wider bandpass. A field instrument would require an interference filter along with an optical system with a greater "throughput" than is possible with the grating assembly used in the laboratory tests.

The minimum detectable thickness of NO for a GFC field instrument monitoring stacks of interest would probably vary from less than 0.005 atm cm to more than 0.1 atm cm. The smaller value corresponds to a stack of known temperature with little or no H_2O in its effluent. The larger value corresponds to large stacks with 100 atm cm of H_2O in the plume at an unknown temperature. These estimates are based on a GFC instrument operating in a single spectral interval and located between approximately 100 m and 200 m from the plume. It is also assumed that the H_2O content of the effluent can be estimated by other methods and that no effluent gases other than H_2O produce any significant interference. In addition, it is assumed that the continuum emissivity due to particulate matter is less than about 0.1. Performances somewhat better than those indicated above could probably be realized by making similar sets of measurements in two or more spectral intervals in which the relative emissions by NO, H_2O, and the continuum are different.

SECTION IV

RECOMMENDATIONS

Although the ultimate accuracy of a remote, passive NO monitor of the type considered here may be limited seriously under certain conditions, its application to less severe conditions should be investigated further. For many applications of remote sensing, errors as large as $\pm$ 20% may be acceptable. Gas-filter correlation instruments appear to be capable of $\pm$ 20% accuracy. Furthermore, no other type of simple NO monitor appears to have more promise for the near future than does the GFC type described in this report. Recommendations for additional investigations and further development of a GFC instrument are listed below under two sub-headings: (1) analytical, and (2) laboratory and field tests.

ANALYTICAL

A field instrument that contains the same basic components as the one employed in the laboratory experiments of this investigation should serve as the basis for several calculations. A preliminary design of the instrument should be made with mirrors, choppers, apertures and detectors of the sizes and in arrangements that would be practical for a field instrument. Two 1-cm long GFC's should be assumed with 1 atm of NO in one cell and 0.1 atm of NO in the other. The spectral filter should pass the spectral interval between 1896 and 1907 cm^{-1}; the average transmittance assumed for the filter should be consistent with multi-layer interference filters that can be fabricated for this spectral interval. Such an interference filter would necessarily replace the complex grating assembly employed in the work reported in Section VII. The detector employed in the design should be liquid-nitrogen cooled InSb with a detectivity within the present state-of-the-art. The minimum detectable amount of NO as imposed by the detector noise should be calculated for the instrument for various samples of NO + N_2 at temperatures between approximately 400 K and 460 K.

Values of radiance for samples consisting of different amounts of NO and at different temperatures can be obtained from the experimental data presented in Section VII. The values of the minimum detectable amount of NO calculated in this manner do not account for interference by H_2O and continuum emission and, therefore, represent the most optimistic instrument performance. In order to estimate more realistic performance, typical concentrations of H_2O and typical emissivities of particulate matter should be assumed. Data given in Section VII on the interference by continuum emission and by H_2O should then be used with the typical amounts of interfering materials to estimate the degradation in the performance of the assumed field instrument. By comparing the estimated performance with the

EPA requirements, it would be possible to determine the types of stacks and situations for which the instrument could be applied. The estimated performances should be compared with those for other methods of remote monitoring that are available, or might be available in the foreseeable future, to the EPA.

A few modifications to the basic instrument could also be considered for additional analytical work. One possible modification involves replacing the opaque, multi-blade chopper with a combination of a GFC and rotating mirrored chopper. This could be adjusted to make the instrument sensitive only to radiant energy of wavelengths near the strong NO lines. The other two GFC's would still be employed in the same manner, but the amounts of NO in each would need to be changed. Improved discrimination against interference by H_2O and continuum emission could probably be achieved by this more complex scheme.

A different possible modification involves using two different spectral bandpasses. The relative sensitivities of the instrument in the two different bandpasses to temperature, H_2O concentration and NO concentration would be different. Thus, the two sets of measurements could improve the accuracy to which the interferences could be accounted for and the NO concentration could be determined.

LABORATORY AND FIELD TESTS

It is probable that the performance of a remote sensor for NO of the type discussed here is limited by interferences. The amount of the interference can not be determined accurately in the laboratory or analytically. Therefore, a few field tests should be performed on typical stacks to obtain additional information on the magnitude of the interferences and to gain practical experience in accounting for them. The first set of recommended field tests should be performed with a simple prototype instrument of the type recommended above for further analytical work. The instrument should employ an interference filter that passes a single spectral interval, approximately 1896 to 1907 cm^{-1}. Two GFC's, with approximately 0.1 atm cm of NO in one cell and 1 atm cm in the other, should be incorporated along with an attenuator on a mechanism that periodically alternates each of these three components into the monitoring beam. The detector signal should be processed, as suggested in Section V, in such a way as to compare the three levels of energy reaching the detector during the times that the two different cells or attenuator are in the beam.

The first field tests should be performed on a typical stack that can simultaneously be monitored by other methods to obtain comparison data on gas temperature, emissivity due to continuum, H_2O concentration and NO concentration. Interpretation of the data would be simplified if different ones of these parameters could be varied independently and if the instrument could be located within a few meters of the stack to reduce absorption by H_2O in the atmospheric path. A series of measurements made at different distances from the same stack would also provide information on interference by atmospheric H_2O.

Additional laboratory tests made under controlled conditions can provide more information that would be valuable in designing a field instrument. The emphasis for laboratory tests should be on ways to minimize interference and on ways to account for it. The results of the recommended analytical work and preliminary field tests should provide the basis for the additional laboratory work.

SECTION V

ILLUSTRATION OF THE SPECTROSCOPIC PRINCIPLES OF REMOTE SENSING BY USE OF A SIMPLE ANALYTICAL MODEL

INTRODUCTION

This section deals with some of the fundamental spectroscopic and radiometric principles involved in passive, infrared methods of remote sensing of pollutant gases in the hot effluent from stationary sources. The discussion is limited to samples of unknown temperature that may include emission by an unknown amount of continuum in addition to the emission by gas species x. All of the results presented in this section have been calculated on the basis of a simple, single-line spectral model that is similar to a very narrow portion of the infrared spectrum of NO. A real instrument would pass a spectral band wide enough to contain several NO lines; however, the simpler model used here is adequate to illustrate some of the problems involved and some of the limitations. The mathematics involved in the single-line calculations is easy to follow, and many of the conclusions reached with the single-line model can be applied directly to the real spectrum.

In addition to illustrating the principles, this section also provides the basis for the experimental measurements and the methods of data reduction that are discussed in subsequent sections of this report. Because of the many parameters involved in relating a series of simple measurements to the concentration of the pollutant gas, the principles can be described best by holding several of the parameters constant while systematically varying a few of the others. Analysis of the data involves accurate determination of relatively small differences between two or more measurable quantities. By employing an analytical model, the small differences can be calculated precisely, making it possible to observe their influences on the values of concentration that are determined.

The response of an instrument to a constant-pressure sample with optical path length ℓ of gas species x at concentration C is a function of the temperature and the product $C\ell$. We assume that ℓ can be determined by other methods and that the temperature of the sample is uniform over the volume being observed. The instrument being considered, and on which the calculations are based, is illustrated conceptually in Figure 1. The instrument employs a series of one or more GFC's used as spectral filters; each GFC contains a different absorber thickness, w, of gas species x. Collecting optics that are normally a part of an instrument of this type are not included in the conceptual diagram of Figure 1. The discussion of Section V does not include problems related to: interference from emission by gases other than species x in the sample, absorption by the atmospheric path between the sample and the observer, or emission by atmospheric gases, clouds or other objects in the background. It is assumed that the

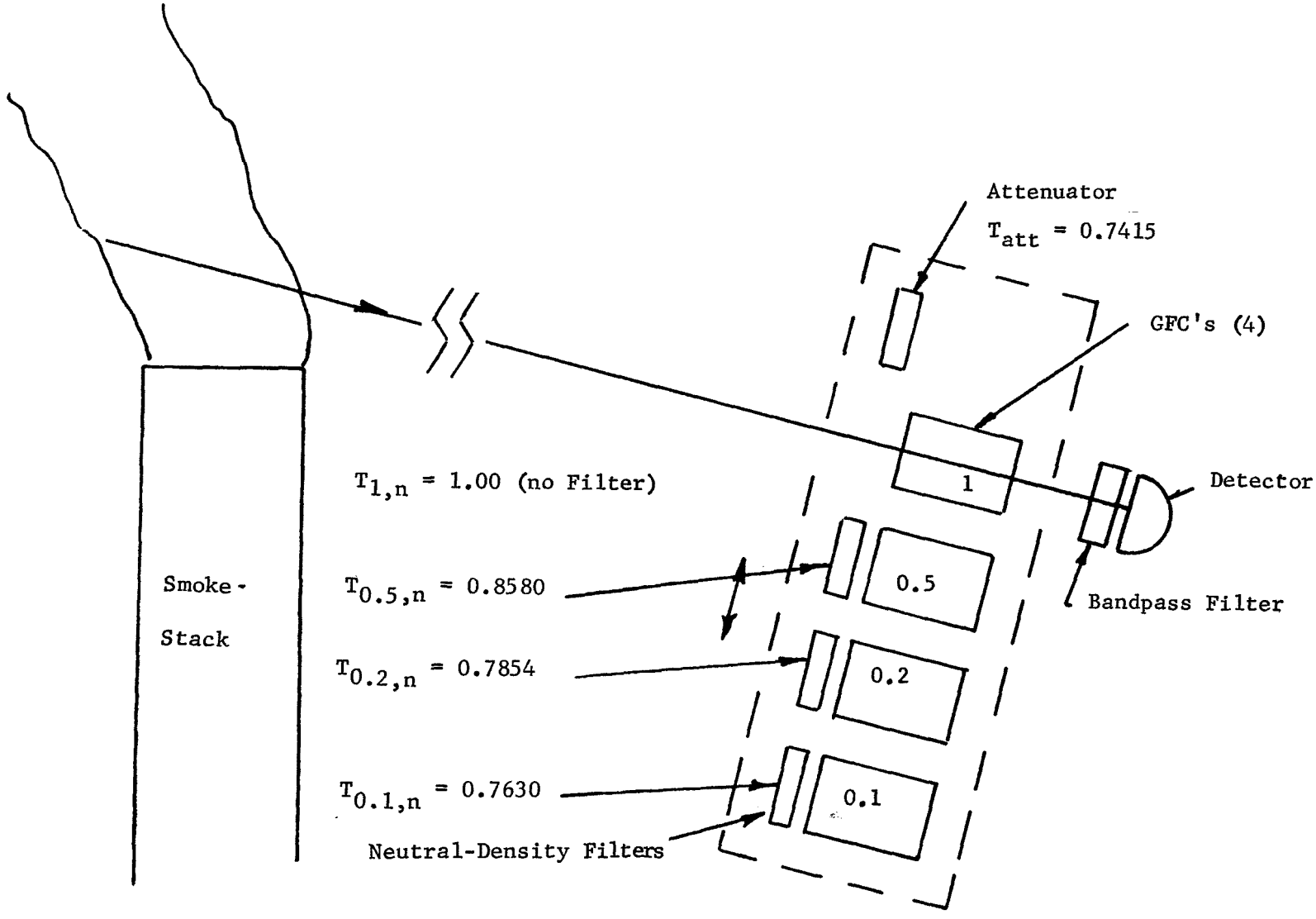

Figure 1. Optical schematic diagram of an instrument of the type on which the calculations of Section V are based. The GFC's are each 1 cm long and are identified by the pressure of pure gas of species x contained in them. The attenuator and the GFC's with their associated neutral-density filters are mounted on a movable assembly so that either GFC or the attenuator can be inserted into the beam.

spectral bandpass is fixed and that the instrument has been calibrated; i.e., the relationship between detector response and the power incident on the detector is known.

SPECTRAL MODEL AND INSTRUMENT PARAMETERS

Figure 2 shows the spectral plots of transmittance of each combination GFC and filter. We assume that the bandpass filter limits the spectral band from the center of the line to a point 1.5 cm^{-1} from the line center. Each line is symmetrical about its center; therefore, the opposite side of the line need not be considered when calculating the average transmittance or the average emissivity. It also follows that calculations of average transmittance, or average emissivity, based on this simple model would also apply under some conditions for a spectral band consisting of many identical lines with the center of each line separated by 3 cm^{-1} from the adjacent ones. The simple, single-line model obviously cannot be applied to a many-line band when the pressure or absorber thickness is high enough that there is significant overlapping of adjacent lines. The restriction of little or no overlapping of lines is not particularly severe for the present application because there is little overlapping of adjacent NO lines for the spectral intervals and absorber thicknesses of interest.

The GFC shown in Figure 1 with the most gas contains one atm cm of gas species x; the transmittance curve of the gas is illustrated by curve D of Figure 2. This GFC has no neutral-density filter associated with it so that $T_{1,n} = 1$. (The subscript 1 identifies the GFC by the absorber thickness, w, of the gas, and the n refers to the neutral-density filter for that GFC. The subscript j is used as a general index to indicate the GFC identified by that letter. The subscript g is used below to indicate the transmittance of the gas in a particular GFC.) The filters associated with each of the other three GFC's are adjusted to provide the same average transmittance of the gas-plus-filter combination as the GFC containing 1 atm cm of gas. The attenuator also has this same transmittance. Thus each correlation cell, or the attenuator, transmits the same energy from a blackbody source to the detector.

The following equations show this relationship and define the various transmittances.

$$T_{att} = \bar{T}_1 = \bar{T}_{0.5} = \bar{T}_{0.2} = \bar{T}_{0.1} = 0.7415, \quad (1)$$

where

$$\bar{T}_{0.5} = \overline{T_{0.5,g}\, T_{0.5,n}}, \quad (2)$$

$$\bar{T}_{0.2} = \overline{T_{0.2,g}\, T_{0.2,n}}, \quad (3)$$

$$\bar{T}_{0.1} = \overline{T_{0.1,g}\, T_{0.1,n}}. \quad (4)$$

Using these adjusted filters with the three GFC's simplifies the analysis of

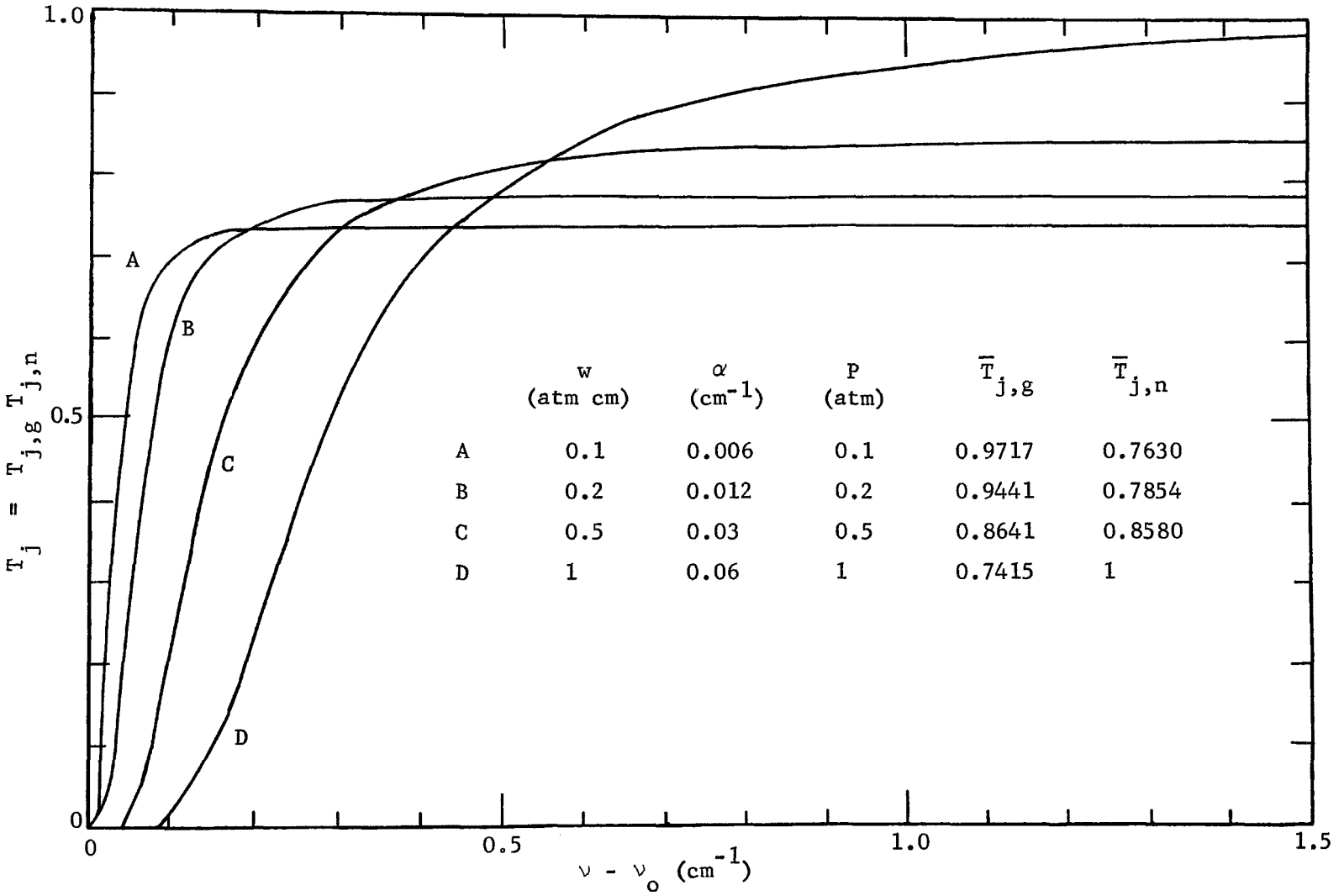

Figure 2. Plot of transmittances of GFC and neutral-density filter combinations. Each combination has the same average transmittance, 0.7415.

the data. In a real instrument they would not necessarily be equal because a different gain factor could be used when reducing the data for each GFC. However, the gas concentration is related directly to the differences between the detector signals, so there are some instrumental advantages in keeping the differences small when there is no absorbing gas in the sample.

The intensity, S, and half-width, α, of the model line used in the calculations are:

$$\begin{aligned} S = \int k \, d\nu &= \pi \text{ (atm cm)}^{-1} \text{ cm}^{-1} \text{ at 300 K} \\ &= 300 \, \pi/\theta \text{ (atm cm)}^{-1} \text{ cm}^{-1} \text{ at other } \theta \\ &= 0.030 \, \pi/\theta \text{ (ppm} \cdot \text{m)}^{-1} \text{ cm}^{-1}, \end{aligned} \tag{5}$$

where k is the absorption coefficient for the single line.

$$\alpha = 0.06 \, P \, (300/\theta)^{0.5} \text{ cm}^{-1} \tag{6}$$

where P is the total pressure in atm.

The value of π was chosen for the intensity S because it simplified some of the calculations and is similar to that of the strongest NO lines. The results can be applied to other values of S by adjusting the values of absorber thickness because the absorption is a function of the product of line intensity and absorber thickness.

We note from the curves in Figure 2 that all of the GFC's are opaque at the center of the NO line. However, the GFC with 0.1 atm cm is strongly absorbing only over a region very near the line center. The absorption by the gas increases as the amount of gas in the GFC is increased. The transmittance of the filter, indicated by $T_{j,n}$ is necessarily smallest for the correlation cells containing the least amount of gas. Essentially all of the absorption indicated by curve A for $(\nu - \nu_o)$ greater than approximately 0.1 cm^{-1} is due to the neutral-density filter associated with the 0.1 atm cm correlation cell.

SPECTRAL EMISSIVITY AND RESPONSE FOR SAMPLES WITH NO CONTINUUM

Figure 3 shows plots of the spectral radiance of two representative samples at two different temperatures, 450 and 410 K. The value of u for the 410 K sample has been adjusted so that the total radiance over the 1.5 cm^{-1} interval is the same for both samples. Values of N_ν^B, the spectral radiance of a blackbody at the sample temperature, are based on 1900 cm^{-1} and are assumed to be constant over the narrow interval used in the calculations. Because of the strong dependence of blackbody radiance on the temperature for the temperatures and wavenumbers of interest, a considerably larger value of u is required for the lower temperature sample.

The values of u for these two samples are probably as large as, or larger than, the largest values of NO that would be measured with the proposed instrument.

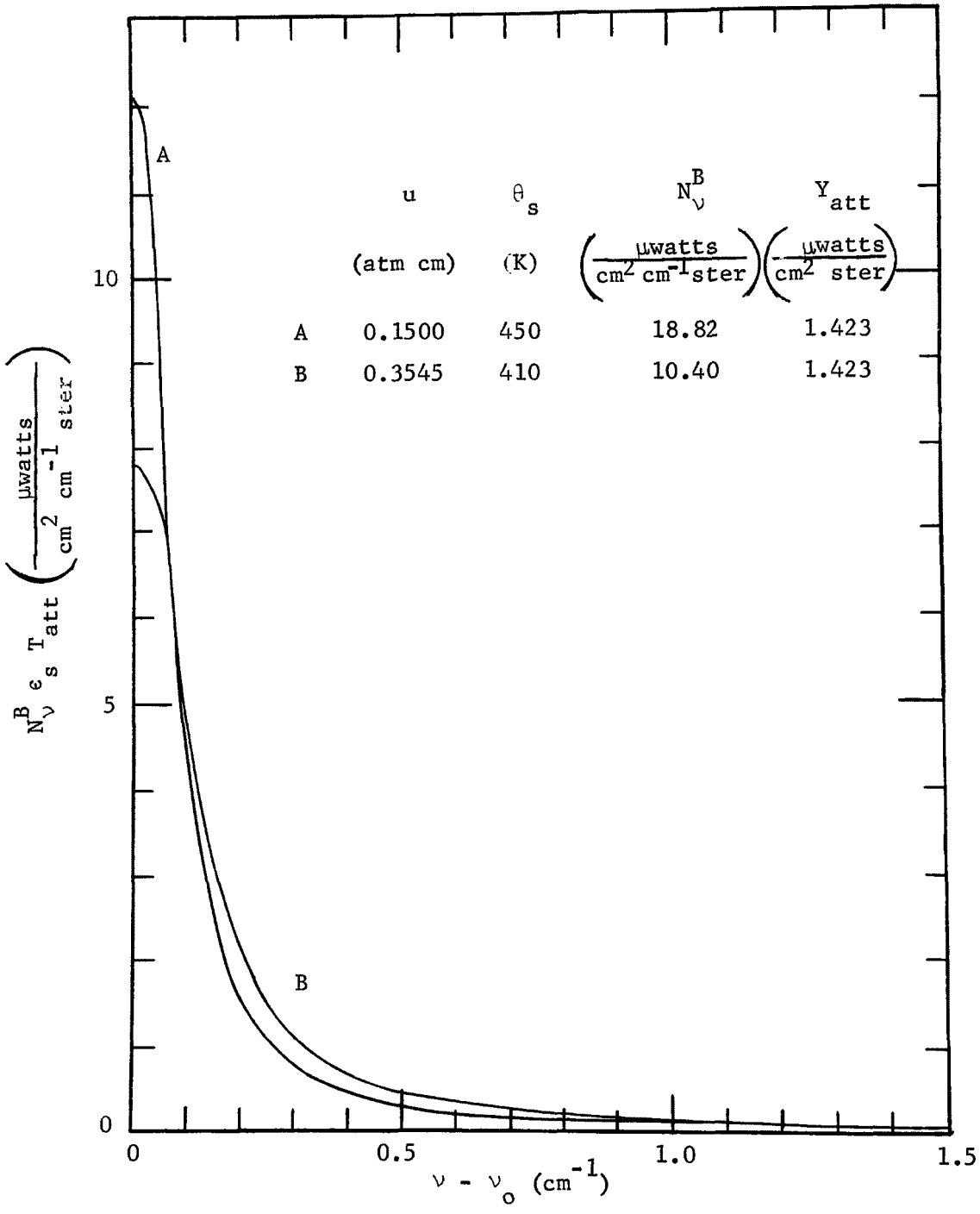

Figure 3. Plots of $N_\nu^B \epsilon_s T_{att}$ vs $(\nu - \nu_o)$ for two samples with ϵ_s in the non-linear region near the line center. The emissivity ϵ_c of the continuum in the sample is assumed to equal zero. $T_{att} = 0.7415$.

The values plotted in Figure 3 represent the beam after it has passed through the attenuator. The spectral radiances of the samples are equal to the values plotted divided by 0.7415, the transmittance of the attenuator.

The power incident on the detector when GFC-j is in the beam is given by the following equation if there is no absorption in the intervening atmospheric path.

$$E_j = M \int N_\nu^B \epsilon_s T_j \, d\nu = M Y_j \qquad (7)$$

The "geometrical" factor M accounts for the length of the optical path between the emitting gas and the detector and for the sizes of the detector and the collecting optics. In most of the discussion that follows, it can be assumed that M remains the same so that E_j is proportional to the calculable Y_j.

The area under each curve of Figure 3, $\int N_\nu^B \epsilon_s T_{att} \, d\nu = Y_{att}$, is proportional to the energy incident on the detector for the corresponding sample of emitting gas. As explained above, ϵ_s for the 450 K sample is made smaller than for the 410 K sample by decreasing u to account for the higher value of N_ν^B for the hotter sample. It follows that a simple radiance measurement cannot distinguish between these two samples, although their concentrations differ by more than a factor of two. If the temperature were known, and if there were no emission by other gases, the NO concentration could, in principle, be determined from the simple radiance measurement. The following discussion explains how, and under what conditions, the GFC's can use the difference in the shapes of the two curves of Figure 3 to determine the concentration without the temperature being known.

Figure 4 shows a pair of curves similar to those in Figure 3 but for much smaller samples. The value of u for the 410 K sample was adjusted so that $\int N_\nu^B \epsilon_s T_{att} \, d\nu = Y_{att}$ is the same for both samples. An instrument would frequently be required to measure thicknesses of NO as small as, or smaller than, those indicated in Figure 4. We note that the two curves in Figure 4 are much more alike than are the two curves in Figure 3. Curve B lies slightly above curve A for $(\nu - \nu_o)$ greater than about 0.05 cm^{-1}, but the small difference can not be seen in the figure. The samples represented by Figure 4 are sufficiently small that the emissivity near the center of the line is much less than unity and is approximately proportional to the absorber thickness u. In contrast, the samples represented in Figure 3 are in the non-linear region so that increases in u do not substantially increase the emissivity near the line centers. Thus, as the value of u is increased to account for decreasing blackbody radiance associated with the decreasing temperature, the spectral radiance increases in the wings of the line at the expense of decreasing radiance near the line center. Because of the similarity of the two curves in Figure 4, it follows that any instrument depending on the spectral characteristics of the radiant energy cannot easily distinguish between the two samples, although they correspond to quite different concentrations of NO.

The emissivities at the center of the line for the four samples represented in Figures 3 and 4 are as follows:

u (atm cm)	0.1500	0.3545	0.0150	0.0257
θ (K)	450	410	450	410
ϵ_s (at ν_o)	0.871	0.994	0.184	0.308

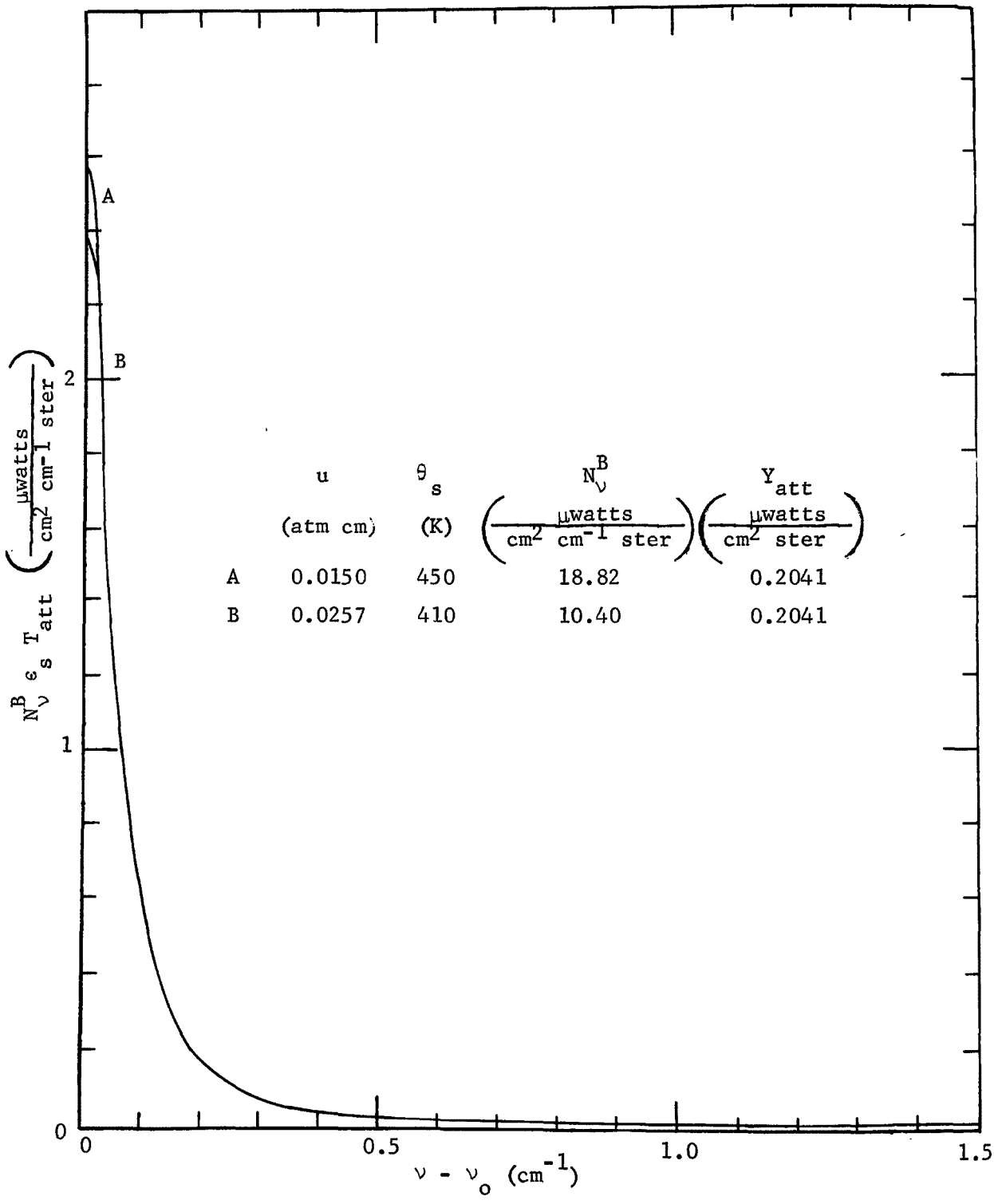

	u (atm cm)	ϑ_s (K)	N_ν^B $\left(\frac{\mu watts}{cm^2\ cm^{-1}\ ster}\right)$	Y_{att} $\left(\frac{\mu watts}{cm^2\ ster}\right)$
A	0.0150	450	18.82	0.2041
B	0.0257	410	10.40	0.2041

Figure 4. Plots of $N_\nu^B \epsilon_s T_{att}$ vs $(\nu - \nu_o)$ for two samples with ϵ_s near the linear region. The continuum $\epsilon_c = 0$. $T_{att} = 0.7415$.

Several of the curves that follow will help in understanding the spectroscopic principles of sensing and of determining concentration for conditions under which the emission by the hot gas is in the non-linear region.

The four curves of Figure 5 present the spectral distribution of the radiant energy reaching the detector for one of the samples listed above. Curve A corresponds to having no GFC or attenuator in the beam; curve B corresponds to the attenuator. The other two curves correspond to the GFC and filter combinations indicated by the value of w. The value of Y_j is proportional to the detector signal for each situation. Because of the correlation between the position of the emitting line and the absorbing line, the GFC with 1 atm cm transmits less than one-fourth of the energy incident upon it. Recall that its average transmittance to blackbody radiation is 0.7415. Note also that the 0.1 atm cm GFC and its associated filter absorb a large fraction of the energy for $(\nu - \nu_o)$ less than 0.05 cm^{-1}. Curves for the other two GFC's (0.2 and 0.5 atm cm) are not shown, but their positions can be estimated on the basis of the curves in Figure 2. It is apparent that each GFC has a strong influence over a different portion of the spectrum; therefore, measurements made with the series of GFC's can provide information about the shape of the emission line.

Figures 6 and 7 show quantities proportional to the spectral radiance for the two samples illustrated in Figure 3 that have the same value of Y_{att}. Figure 6 represents the radiant energy at the detector after it has passed through the 0.1 atm cm GFC. Similarly, the curves in Figure 7 correspond to the 1 atm cm GFC. Values of Y_j, which are proportional to the areas under the curves, are tabulated in the captions of the figures. Note that either GFC absorbs a bigger fraction of the energy emitted by the source at higher temperature and smaller u than of the energy emitted by the low-temperature source.

Figure 8 shows a plot of Y_j vs w, the absorber thickness of gas species x in the GFC's. Curve A corresponds to the 410 K sample represented in the previous figures. The point at w = 0 corresponds to the detector signal when the attenuator is in the beam. The other 4 points on the same curve correspond to Y_j, which is proportional to the detector signal when the four GFC's shown in Figure 1 are in the beam. Curve E corresponds to the 450 K sample represented in previous figures. The other curves correspond to other samples at the temperatures indicated. In every case the value of u has been adjusted to produce a constant value of Y_{att}.

Recall from the discussions of Figures 1 and 2 that Y_j would be the same for all values of w if the emitted radiation were continuous in nature. The difference between Y_{att} and Y_j for any one of the GFC's is a measure of the structure in the spectrum of the emitted energy that is correlated with the structure in the spectrum of the gas in the GFC.

We first consider measuring the value of Y_{att} and assume that for each value of Y_{att} we have available a family of curves similar to those shown in Figure 8. Next, the value of Y_1 is measured. It is possible, in principle, to then determine a unique value of u by interpolating between the curves of the appropriate figure corresponding to Figure 8. It is not necessary to have the complete set of curves of Y_j vs w; only a series of values corresponding to the value of w used is required. Thus, when all of the sample emission is by gas

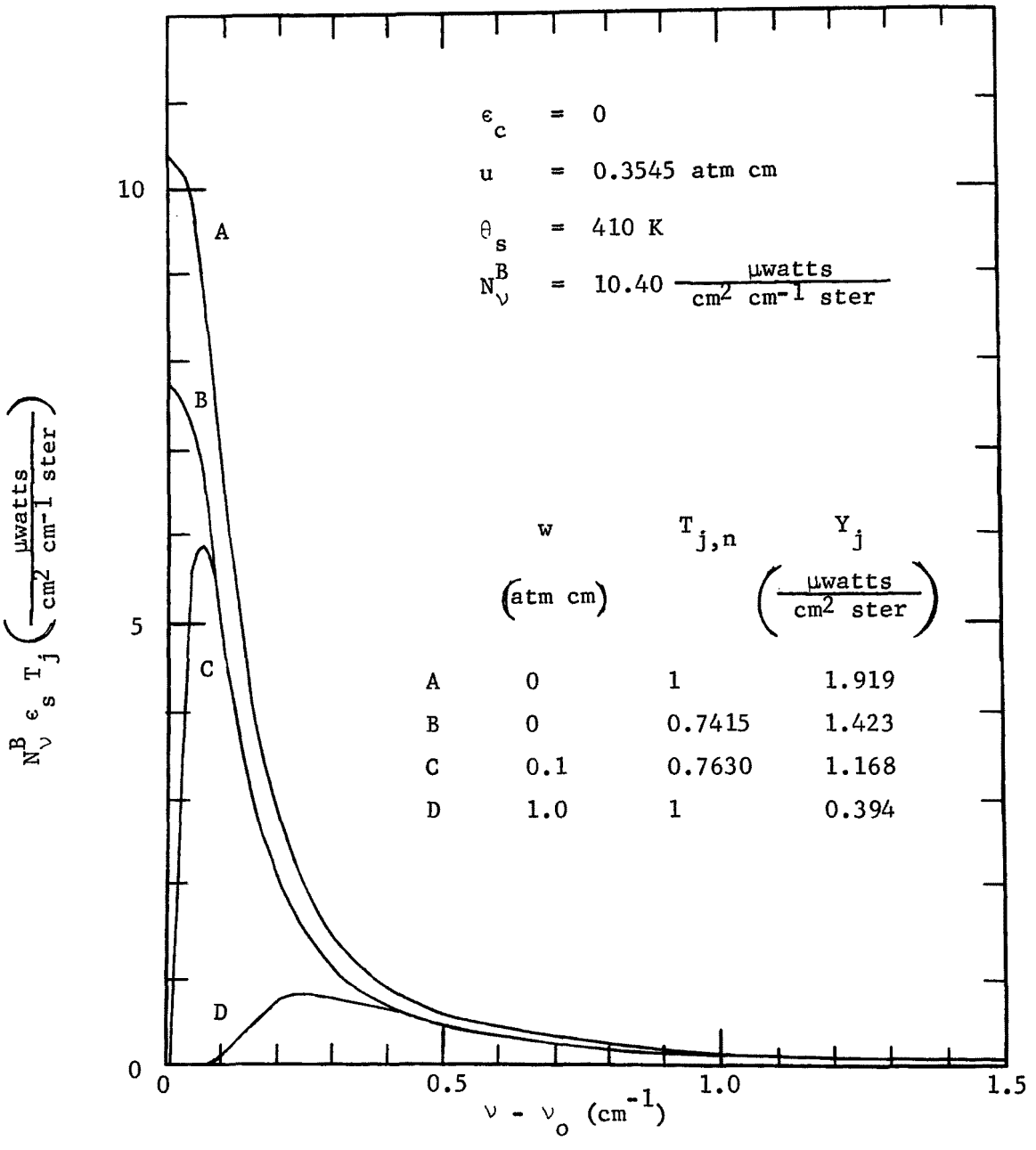

Figure 5. Spectral plots of $N_\nu^B\ \epsilon_s\ T_j$ vs $(\nu - \nu_o)$ for the attenuator and two GFC's. Curve A represents the corresponding quantity with neither an attenuator nor a GFC in the beam.

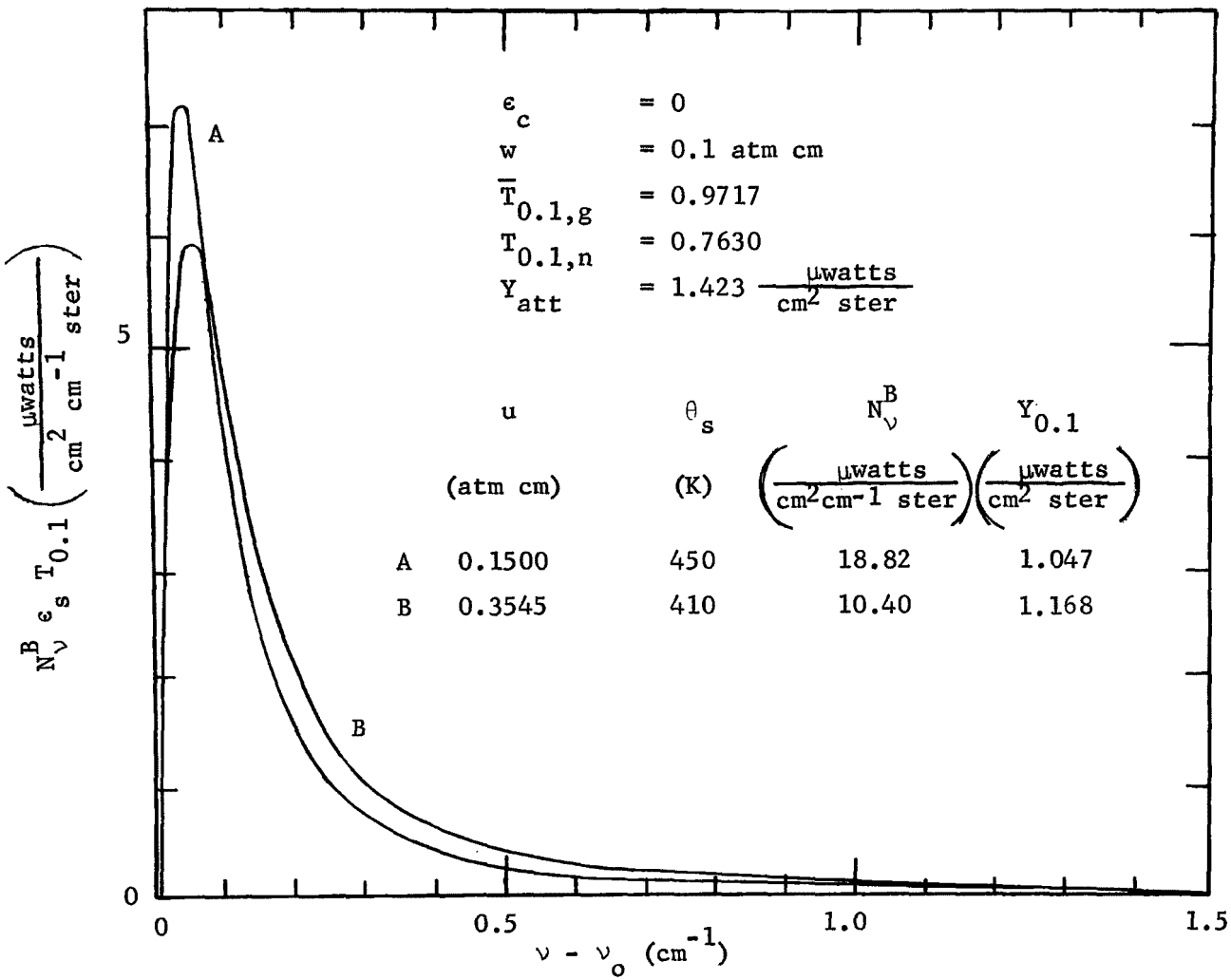

Figure 6. Spectral plots of $N_\nu^B\ \varepsilon_s\ T_{0.1}$ vs $(\nu - \nu_o)$ for two temperatures.

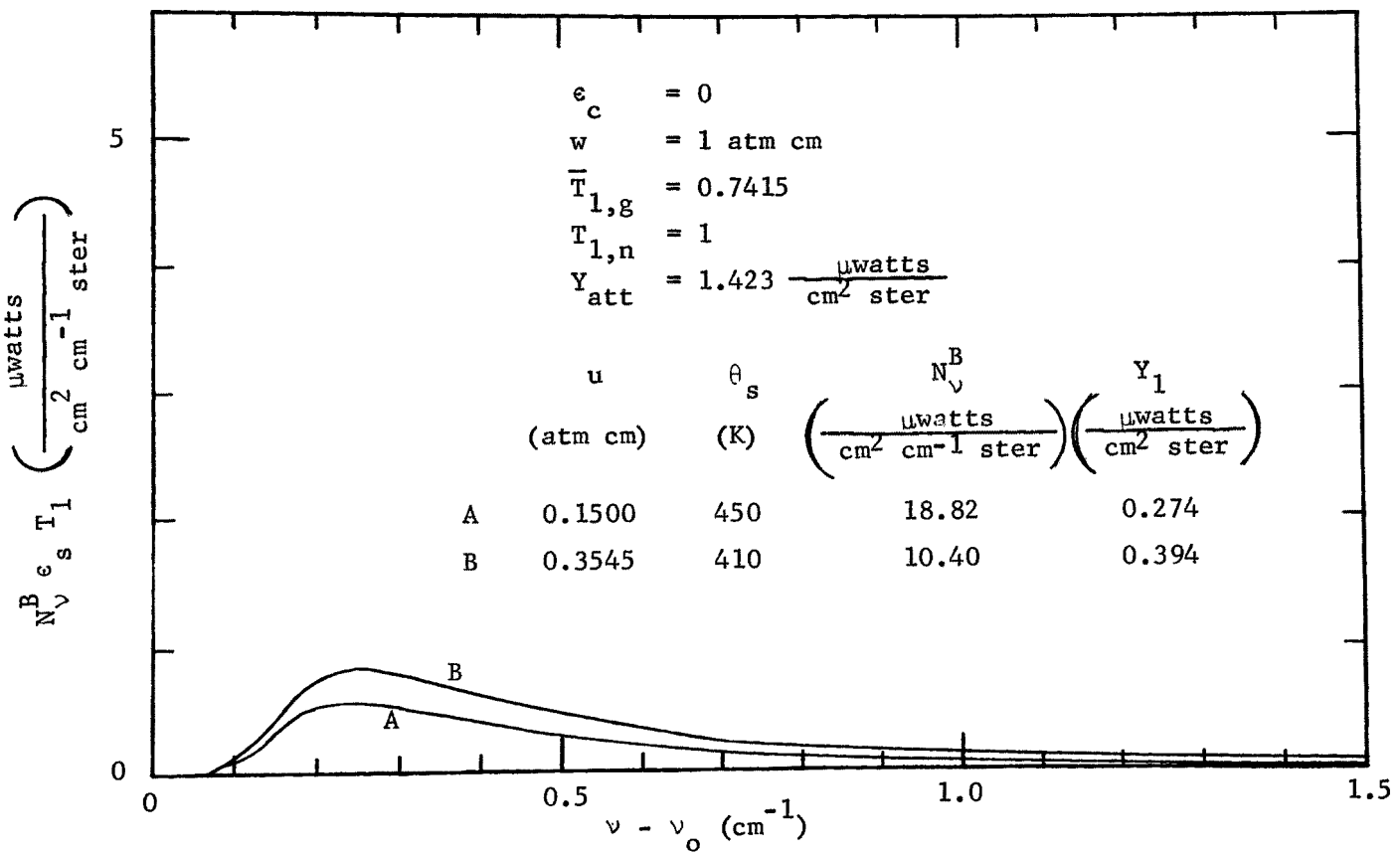

Figure 7. Spectral plots of $N_\nu^B\ \epsilon_s\ T_1$ vs $(\nu - \nu_o)$ for two temperatures.

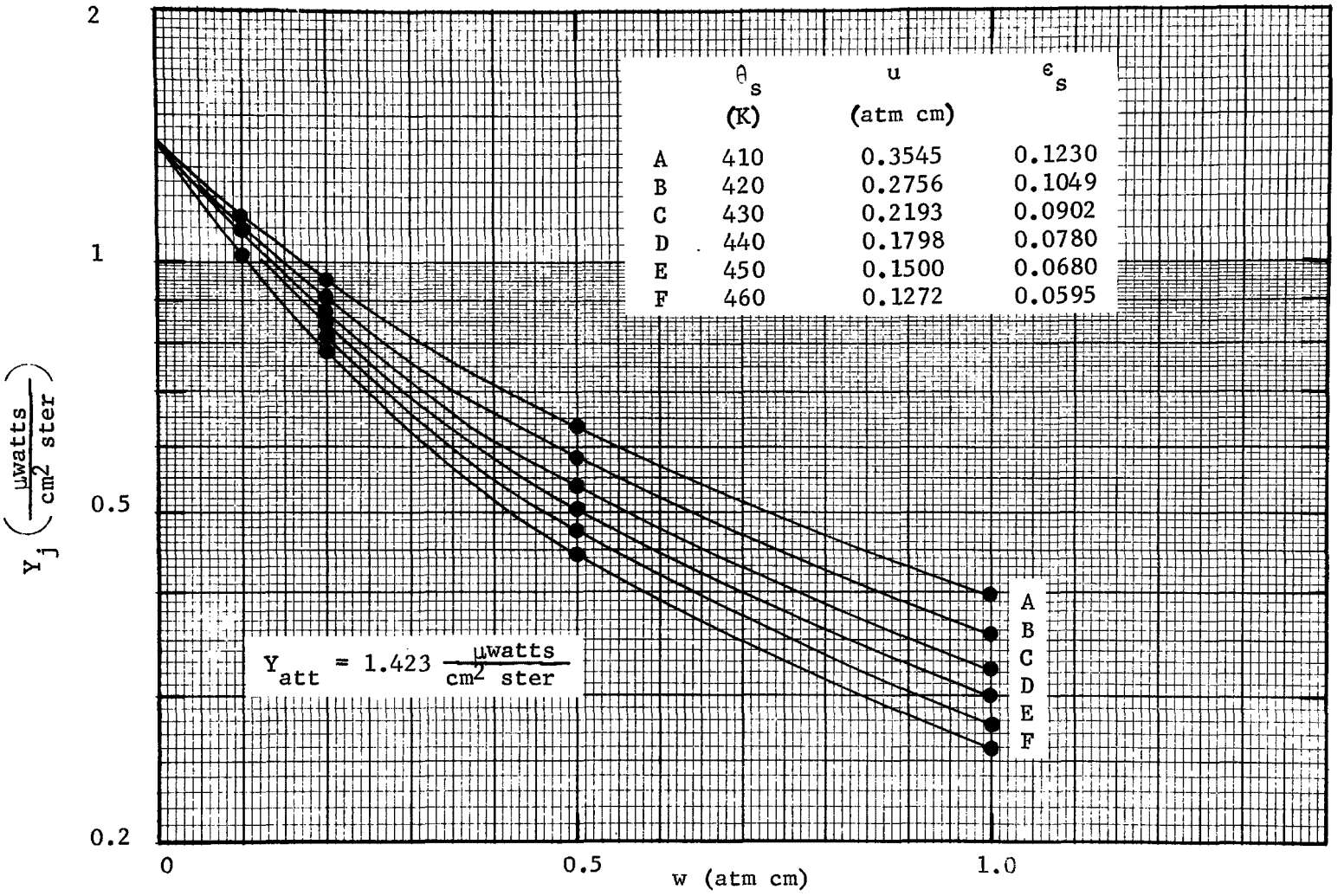

Figure 8. Semi-logarithmic plots of Y_j vs w for various samples. $\epsilon_c = 0$. The points represent the values of w that correspond to the four GFC's illustrated in Figure 1.

species x, the value of u can be determined with only the attenuator and one correlation cell. Measurements made with the other correlation cells would provide additional data and tend to improve the accuracy of the measurement. However, for samples of pure gas of species x with no continuum emission or emission by interfering gases, the value of u can be determined with exact measurements of Y_{att} and Y_j for one of the GFC's. If a single GFC is to be used, it follows that an appropriate value of w must be used for the range of values of u to be measured. The advantage of using more than one GFC will become apparent in later discussions of samples containing continuum emission.

In the discussion of the method of determining concentrations from two measurements, we assumed that we had available a very large number of curves corresponding to those in Figure 8. Each set of curves represented a different value of Y_{att}. The value of Y_{att} is expected to vary over wide ranges, making it necessary to have many sets of calibration curves corresponding to many discrete values of Y_{att}. It would be more convenient to plot the quantity

$$Z_j = \frac{Y_{att} - Y_j}{Y_{att}} \tag{8}$$

The ratio represented by Z_j has a much weaker dependence on the sample temperature or absorber thickness; therefore, fewer sets of calibration curves of this quantity would be required. This ratio is also a measure of the correlation between the spectral structure of the emitting sample and that of the gas in the GFC. For example, if the sample emits continuum energy with no spectral structure, then $Y_{att} = Y_j$, and $Z_j = 0$. In the other extreme, if the GFC is opaque at all wavenumbers where the sample emits, then $Y_j = 0$, and Z equals the maximum value of unity.

Figure 9 shows the data from Figure 8 plotted in a different manner. The ordinant is the ratio above, and the absorber thickness of the sample is the abscissa. Each curve corresponds to a different GFC, each containing one of the different values of w indicated. A set of curves similar to those in Figure 9 would be required for several discrete values of Y_{att}. Interpolation would be performed for values of Y_{att} between those values for which a family of curves is available. Sample temperatures required to maintain the fixed value of Y_{att} are higher than those of interest for values of u less than those represented.

Figure 10 shows another plot for the same data shown in Figure 8. In this figure the sample temperature is the abscissa. Recall that the value of u depends on the temperature because Y_{att} is maintained constant. Thus, from a measurement of Y_{att} and a measurement of Y_j for a properly chosen GFC, we can determine the sample absorber thickness and its temperature. Of course, this is based on the unrealistic assumptions that the sample gas is at a uniform temperature, there is no emission by an interfering gas, there is no continuum emission by particles, there is no interference by the atmosphere, and the measurements can be made with good precision. It is further assumed that the absorber concentration in the sample is sufficiently high that the emissivity near the center of the line is high enough to have a non-linear relationship with the concentration. The remainder of this section deals with conditions under which one or more of these assumptions is not valid.

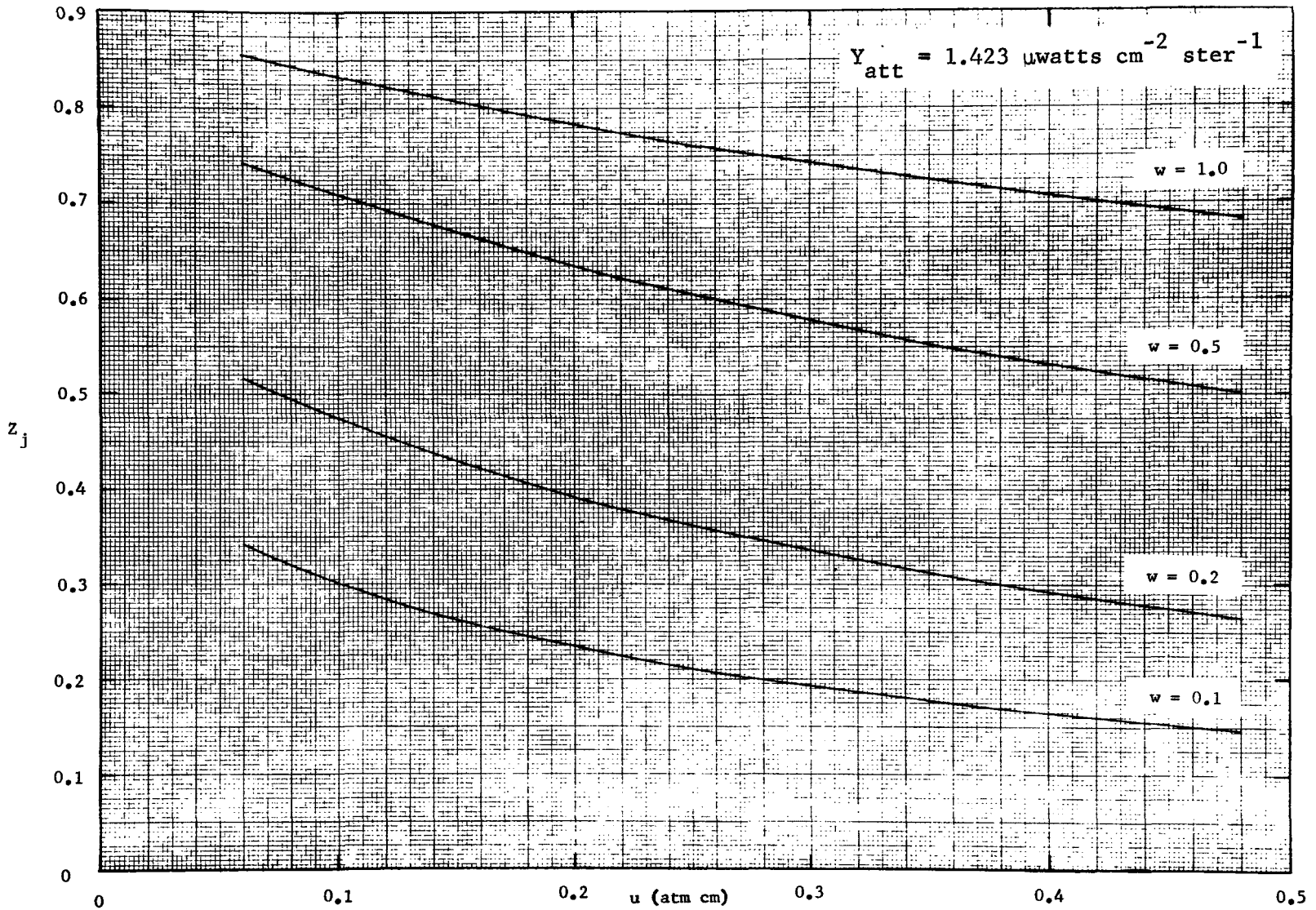

Figure 9. Plots of Z_j vs u for various GFC's. The sample temperatures have been adjusted to maintain Y_{att} = 1.423 μwatts cm^{-2} ster^{-1}. ϵ_c = 0. Values of w are in atm cm.

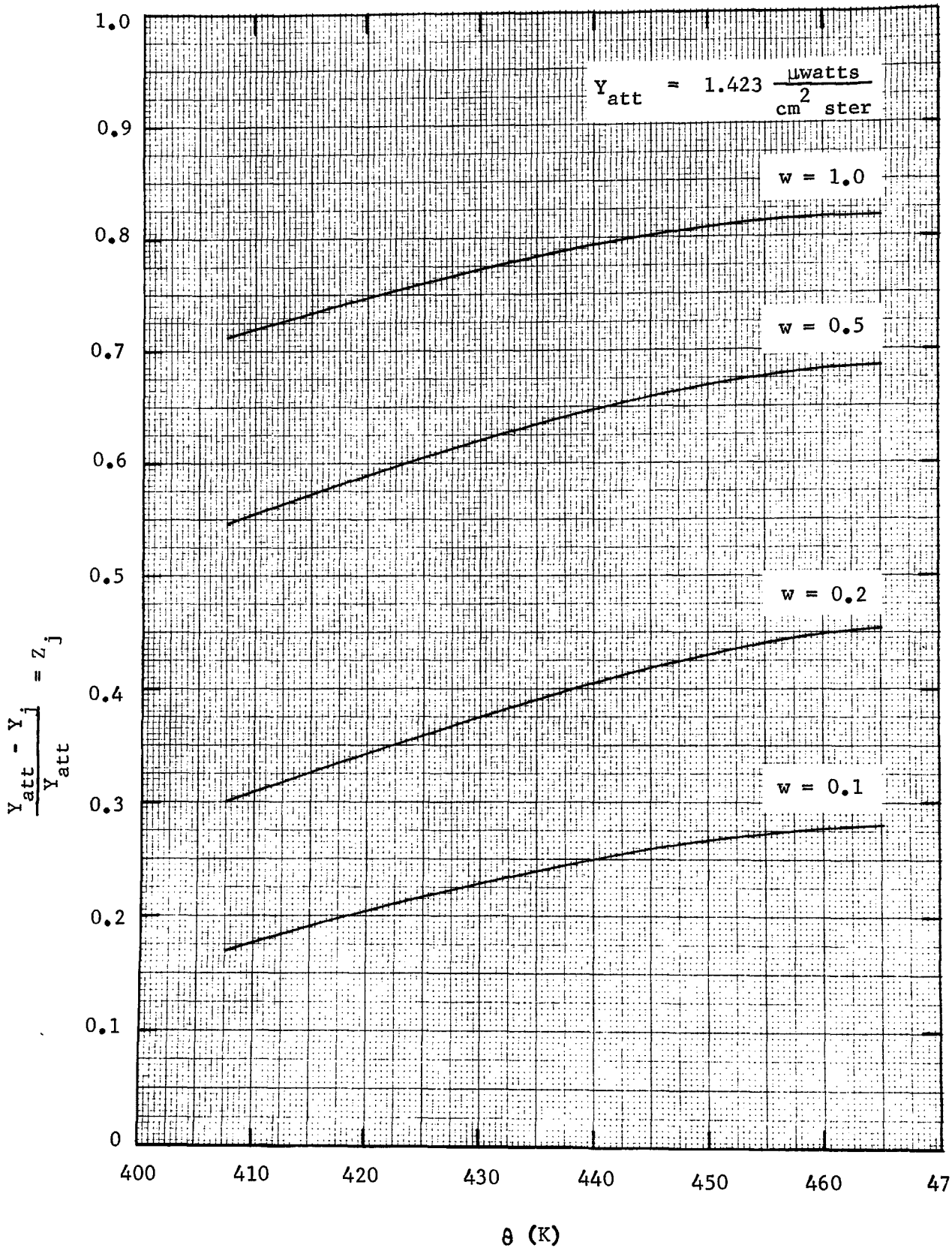

Figure 10. Plots of Z_j vs temperature for various GFC's. Values of u have been adjusted to maintain constant Y_{att} = 1.423 μwatts/cm^2 ster ϵ_c = 0. Values of w are in atm cm.

Figure 11 shows semi-logarithmic plots of Y_j vs w for the relatively small samples represented by Figure 4. The two samples are at 410 and 450 K with the values of u adjusted to provide the same value of Y_{att} for both samples. The two curves of Figure 11 differ by only a small amount; however, the values of u differ by approximately a ratio of 1.6 to 1. Therefore Y_{att} and Y_j for one of the GFC's will both have to be measured quite accurately in order for one to determine u from a family of curves such as the two represented in Figure 11. The relatively weak dependence of the two curves on u could, of course, be predicted from the two curves of spectral radiance in Figure 4. Because of the small difference in shapes of the two curves of spectral radiance, it is to be expected that the radiance measured through any correlation cell would be similar for both samples.

The calculated data presented in this subsection are based on samples with no continuum emission nor emission by gases other than species x. The amount of radiant energy emitted is therefore dependent only on the temperature and the absorber thickness of gas species x. For samples with large enough absorber thickness that the emissivity has a non-linear relationship with absorber thickness, the shapes of the spectral curves of emission are different, making it possible to determine u and θ from two separate measurements. The quantities measured are proportional to Y_{att} and Y_j, where Y_j is measured with a GFC containing an appropriate amount of gas species x. When considering samples that contain continuum emission, the radiance depends upon three quantities: the temperature, u and ϵ_c. Therefore, in order to determine u, it is necessary to make at least three independent measurements of three different quantities, each of which has a different dependence on the three parameters. If the temperature could be determined by some other method, u could be determined, at least in principle, from only two measurements. For the present study, it is assumed that no other method can be depended upon to determine the gas temperature. The following subsection deals with hot gas samples containing continuum emission.

EMISSION BY SAMPLES WITH CONTINUUM

Figure 12 shows three plots of $N_\nu^B \epsilon_s T_{att}$ vs $(\nu - \nu_o)$ for three different samples. Sample A is one of those represented in Figure 3 and is used as a basis for some of the calculations in the other figures. Samples B and C are at the same temperature, 450 K, but also contain enough particles or other source of continuum emission to produce continuum emissivities of $\epsilon_c = 0.02$ and 0.05, respectively. The value of u has been varied to make Y_{att} constant for all three samples. Samples such as those represented in Figure 12 form the basis for several of the following curves used to demonstrate a procedure by which the absorber thickness, or concentration of gas species x, can be determined from a set of three or more measurements.

We assume that Y_{att} is measured first and that a complete set of calibration charts of Z_j vs u are available for many different values of Y_{att}. Interpolation would be required for values of Y_{att} for which no calibration curves are available. In practice, the many sets of calibration curves would probably be replaced by data stored on a simple computer. However, it is better for our present purposes to discuss the analysis in terms of the graphs so that the relationships between the parameters are more apparent. By using the graphs, it is possible to get a better understanding of the accuracy required for each of the measurements in order to obtain the required accuracy in the concentration measurement.

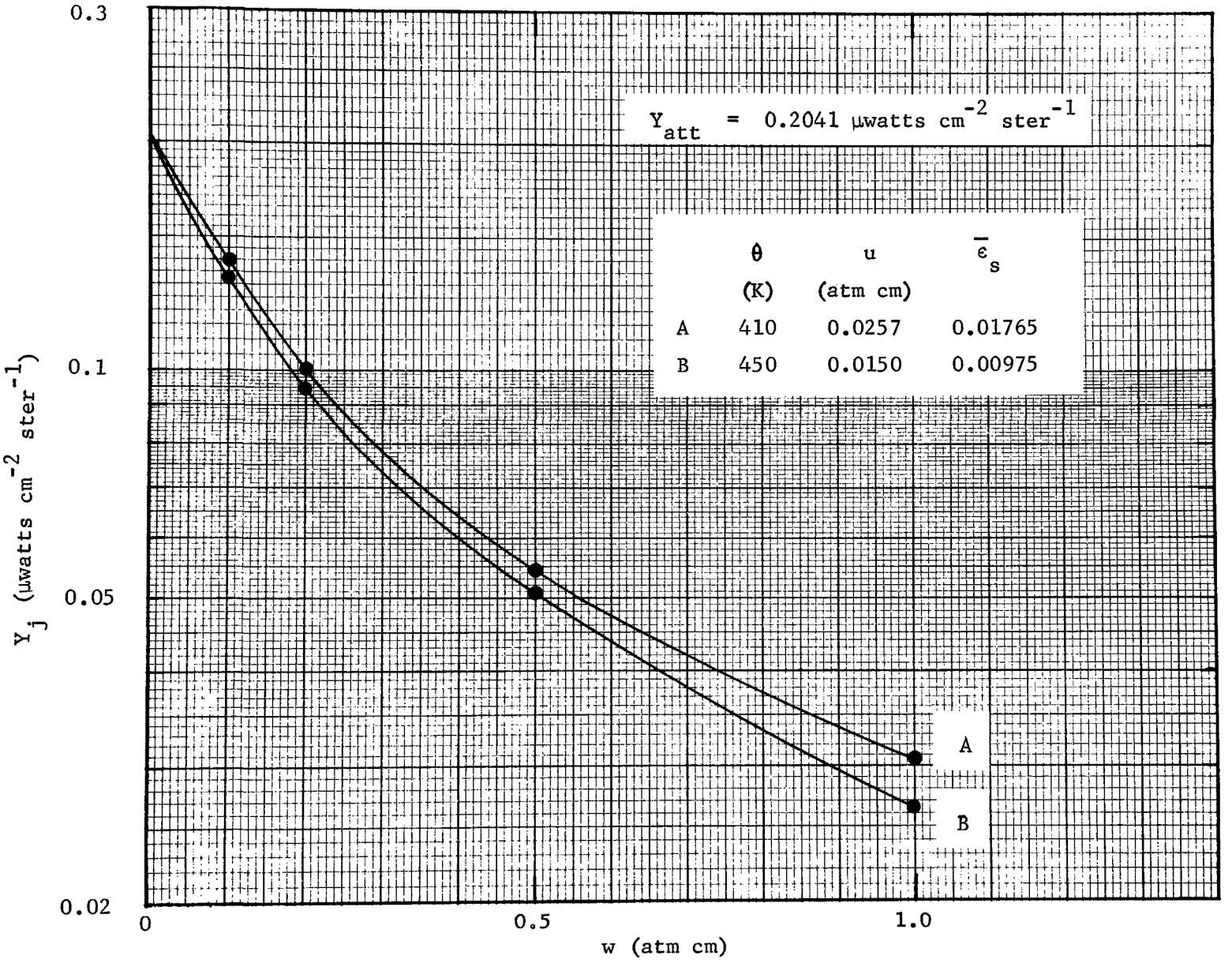

Figure 11. Semi-logarithmic plots of Y_j vs w for two small samples at different temperatures with the same value of Y_{att}.

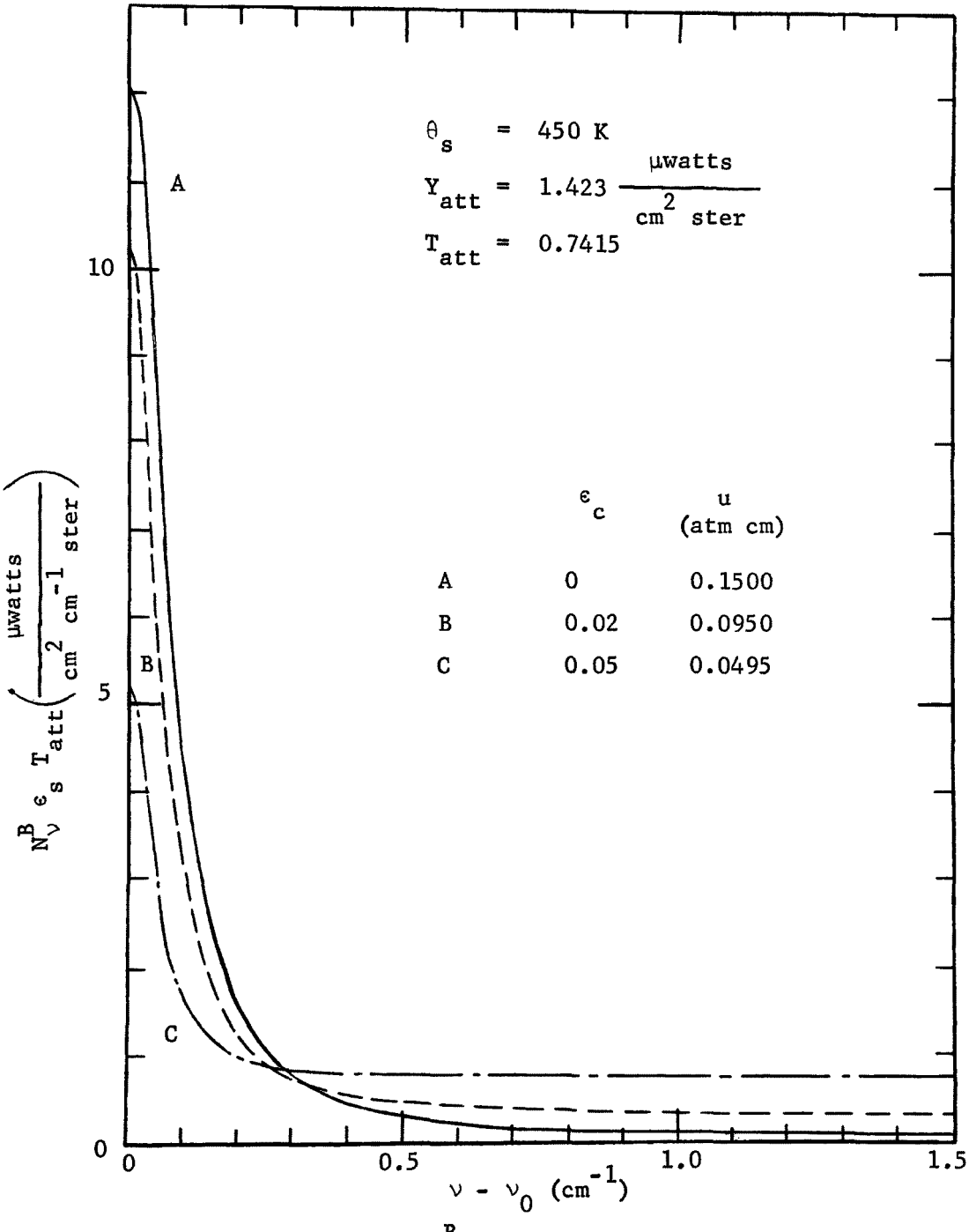

Figure 12. Spectral plots of $N_\nu^B \epsilon_s T_{att}$ for three samples at 450 K. The emissivity of the continuum is as indicated for each curve. The value of u has been adjusted to make Y_{att} = 1.423 μwatts cm^{-2} $ster^{-1}$.

Figures 13 and 14 illustrate the method by which measured values of Y_{att}, Z_1, and $Z_{0.1}$ can be used to determine unique values of ϵ_c and u under certain restricted conditions without an independent measurement of the temperature. The two figures are based on Y_{att} = 1.423 μwatts cm^{-2} $ster^{-1}$, the value that corresponds to the samples illustrated in Figure 12 and in a few of the other figures shown above. Figure 13 represents measurements made with the GFC containing 1.0 atm cm of gas; Figure 14 shows corresponding data for the GFC containing 0.1 atm cm of gas. Each curve in the two figures corresponds to the value of continuum emissivity indicated. As an example, if Y_{att} = 1.423 μwatts cm^{-2} $ster^{-1}$, Z_1 = 0.835 and $Z_{0.1}$ = 0.302, we can see from Figures 13 and 14 that ϵ_c = 0 and u = 0.1 atm cm. As another example, assume that Y_{att} = 1.423 μwatts cm^{-2} $ster^{-1}$, Z_1 = 0.70 and $Z_{0.1}$ = 0.208. The only pair of values that fits the curves of both figures is ϵ_c = 0.01 and u = 0.2 atm cm. The examples given were chosen so that the values of ϵ_c fall on one of the curves. In most cases, it would be necessary to interpolate between the curves to find a value of ϵ_c and a value of u that would produce the two observed values of Z_j. In interpreting the curves of Figures 13 and 14, it is important to recall that each point on a given curve corresponds to a different sample temperature. The ends of the curves that represent small values of u have been omitted because they correspond to temperatures higher than those of interest.

The results corresponding to the other two GFC's (w = 0.5 and w = 0.2 atm cm) are not included. As discussed above, only three independent measurements are required. Therefore, Y_{att}, Z_1, and $Z_{0.1}$ should be adequate. Inclusion of measurements with the other two GFC's could possibly reduce error, but in principle they are not required.

The data in Figures 13 and 14 have been cross-plotted in Figures 15 and 16. The latter two figures provide a different method for determining the values of u and ϵ_c from the data. Each curve represents a given value of Z_j. By interpolatint between the curves for values of Z_j not plotted and by comparing Figures 15 and 16, it is possible to determine a unique set of values of ϵ_c and u. It is apparent from the curves that a small error in Z_j for either GFC can produce a large error in u. After ϵ_c and u have been determined, θ_s can be determined from a set of curves similar to those in Figure 17.

In order to illustrate the errors in u that would result from errors in Z_j, we have made several calculations covering a variety of conditions. Some of the results are summarized in Table 1. In the example represented by the first line, Y_{att} = 0.2041 μwatts/(cm^2 ster), $Z_{0.1}$ = 0.247 and Z_1 = 0.625. From plots similar to those of Figures 13 and 14 that were drawn for Y_{att} = 0.2041 μwatts/(cm^2 ster), we have determined that u = 0.020 atm cm and ϵ_c = 0.005. We then assume that Z_1 was read correctly, but $Z_{0.1}$ was erroneously read as 0.259 instead of 0.247, (see line 2). This realistic 5% error in $Z_{0.1}$ causes the value of u determined from the calibration curves to decrease by 29% from 0.0200 to 0.0142. The third line corresponds to an error of 0.01 (1.5%) in Z_1; 0.635 was read instead of 0.625 the correct value. The first line of each group of three lines represents the correct values. The second and third lines illustrate the errors produced by the erroneous readings as underlined.

The errors assumed in the example above, 0.012 for $Z_{0.1}$ and 0.010 for Z_1, are about equally probable. Note that the error in $Z_{0.1}$ produces a larger error

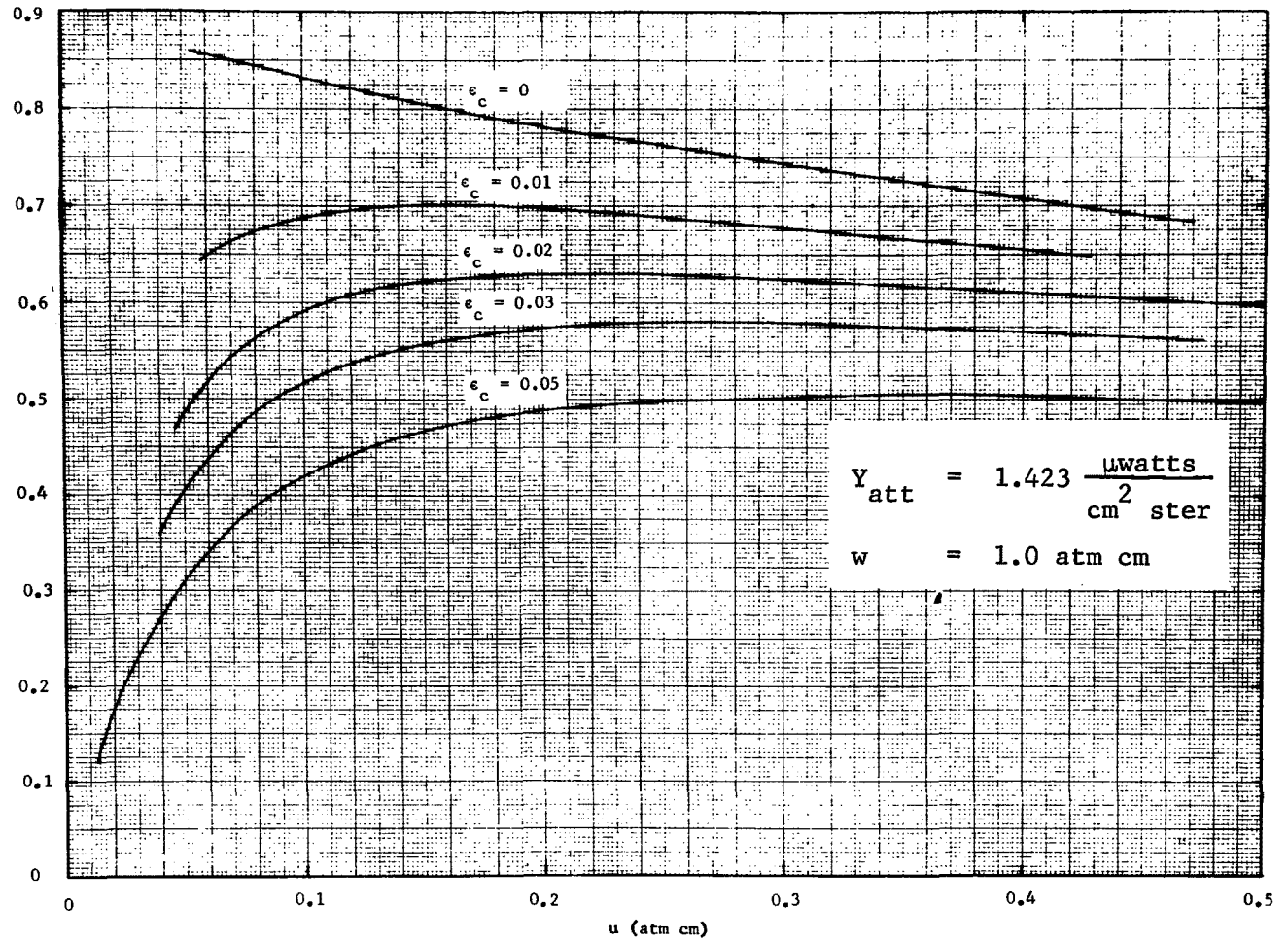

Figure 13. Plots of Z_1 vs u for five different values of ϵ_c.

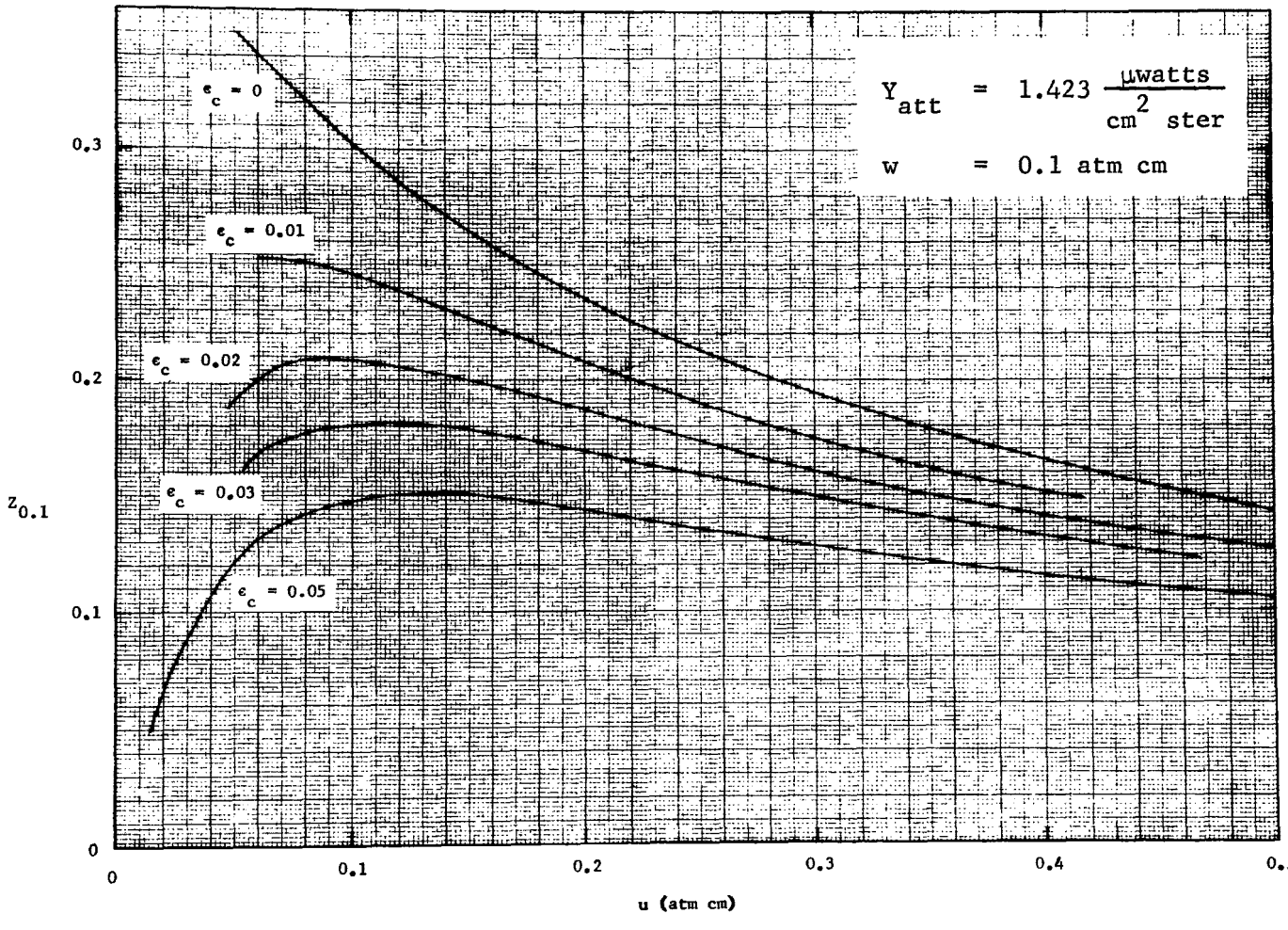

Figure 14. Plots of $Z_{0.1}$ vs u for five different values of ϵ_c.

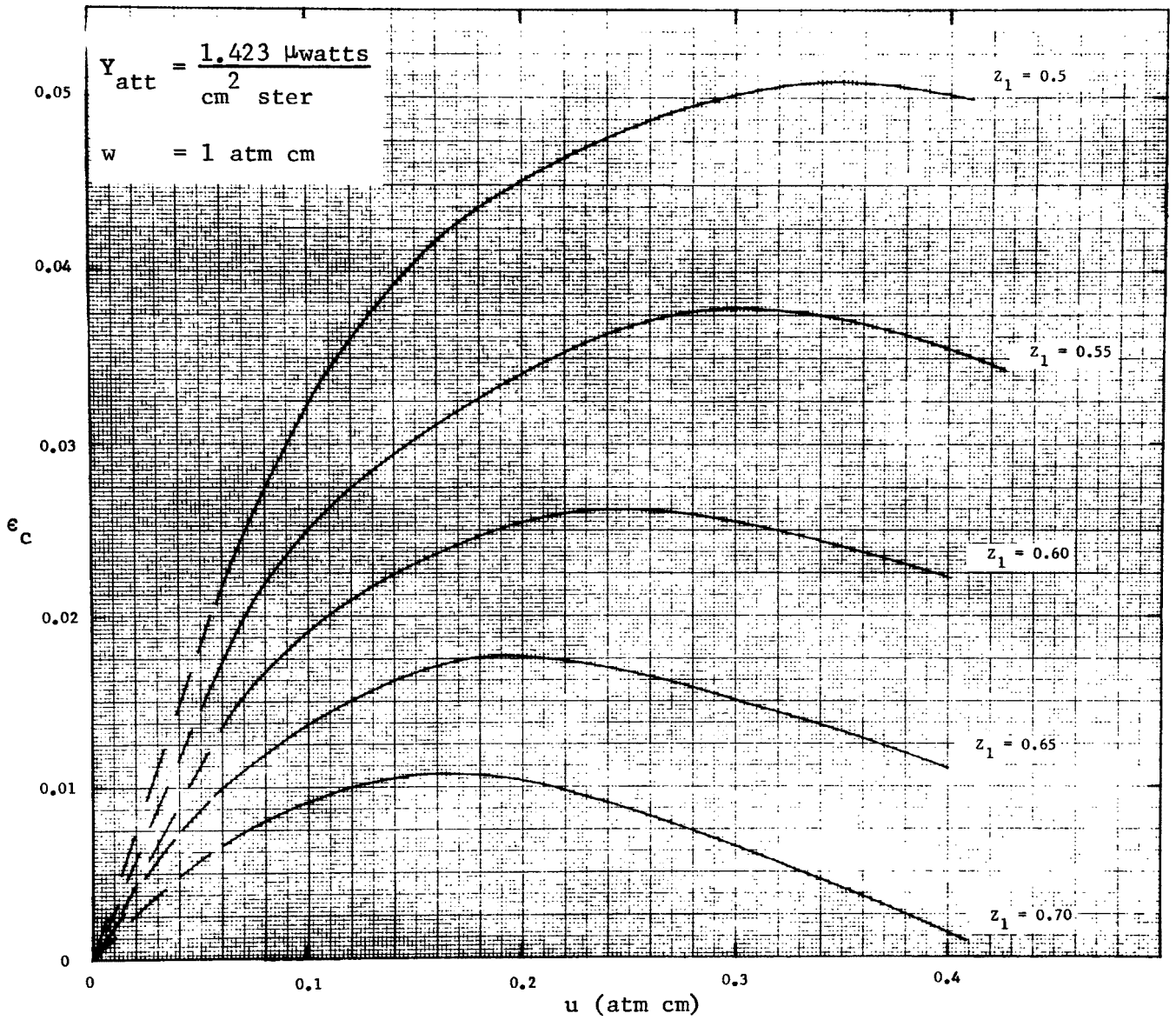

Figure 15. Plots of ϵ_c vs u for five different values of Z_1.

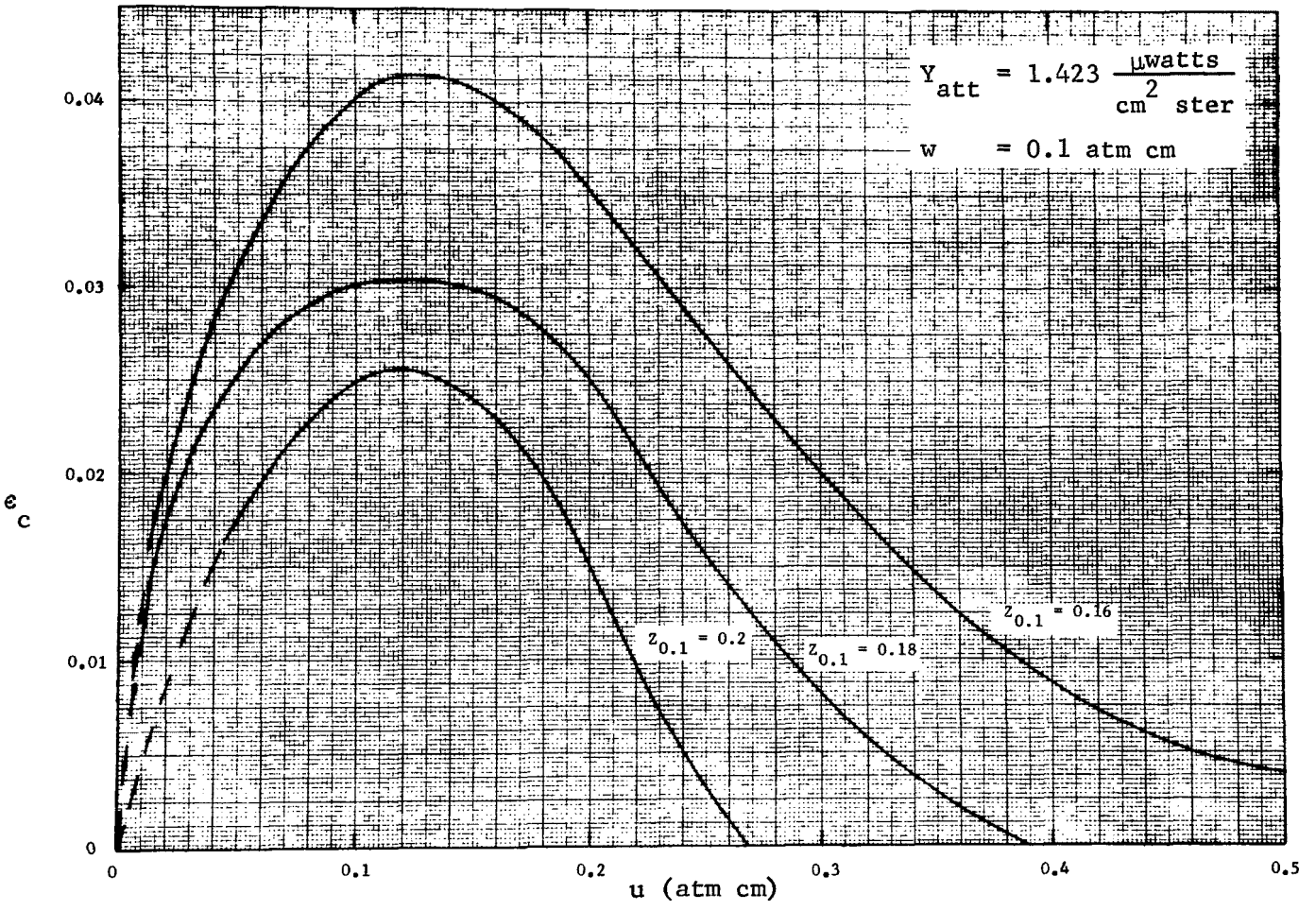

Figure 16. Plots of ϵ_c vs u for three different values of $Z_{0.1}$.

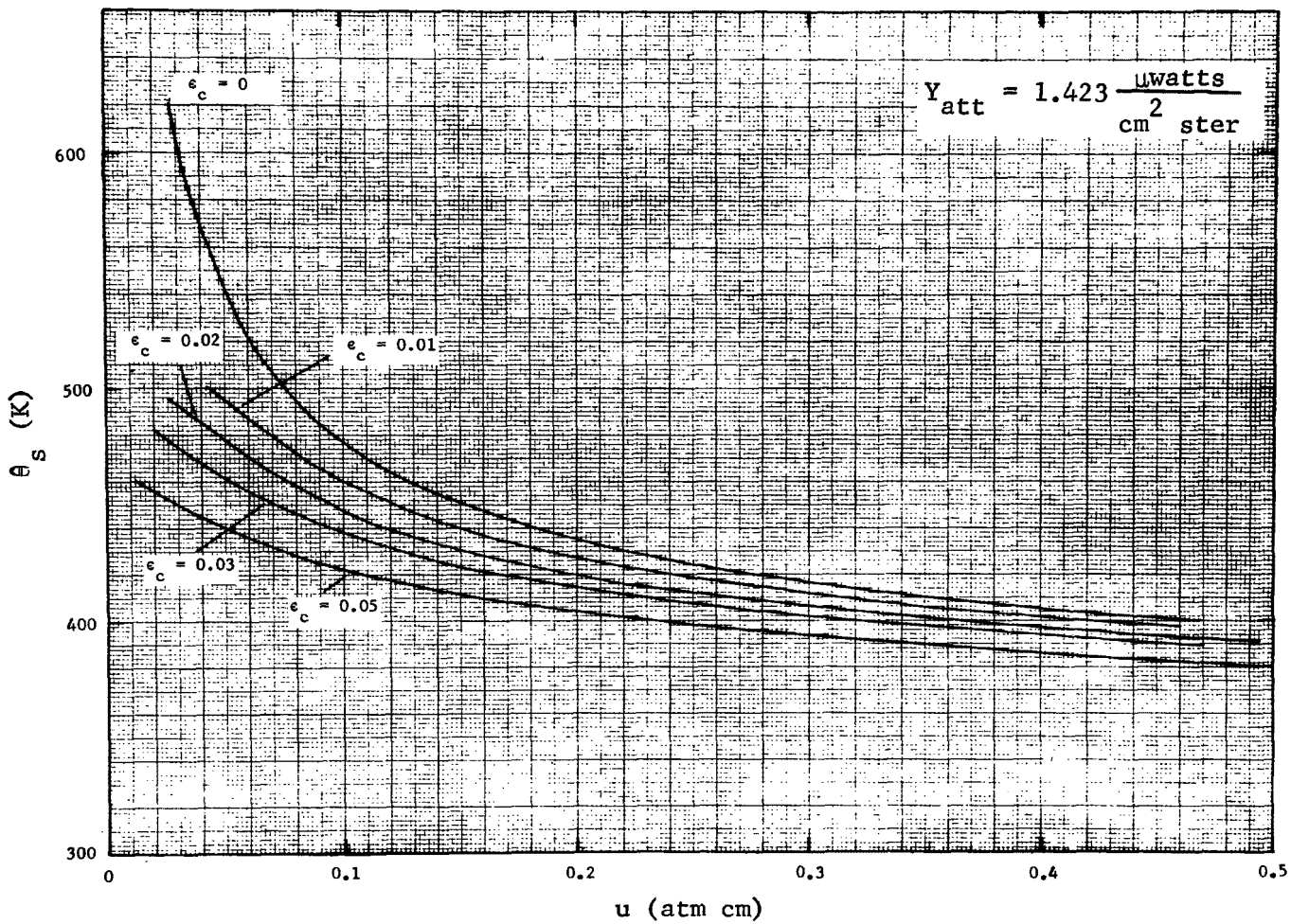

Figure 17. Plots of Θ_s vs u for five different values of ϵ_c. The curves are based on the data in Figures 15 and 16.

TABLE 1

ERRORS IN u DUE TO INCORRECT VALUES OF Z_j

$Y_{att} = 0.2041 \frac{\mu watts}{cm^2\ ster}$

$Z_{0.1}$	Z_1	u (atm cm)	ϵ_c	θ_s (K)	Error in u
0.247	0.625	0.020	0.005	404	
0.259	0.625	0.0142	0.0031	428	29% low
0.247	0.635	0.022	0.00505	400	10% high
0.261	0.710	0.040	0.005	374	
0.274	0.710	0.021	0.0031	407	48% low
0.261	0.720	0.0455	0.00495	370	11% high
0.255	0.735	0.060	0.005	358	
0.268	0.735	0.029	0.0031	392	51% low
0.255	0.745	0.0685	0.0043	376	11% high

$Y_{att} = 1.4234 \frac{\mu watts}{cm^2\ ster}$

$Z_{0.1}$	Z_1	u (atm cm)	ϵ_c	θ_s (K)	Error in u
0.207	0.543	0.070	0.02	457	
0.217	0.543	0.055	0.015	483	21% low
0.207	0.553	0.076	0.0205	459	9% high
0.208	0.592	0.100	0.02	446	
0.218	0.592	0.0835	0.0148	462	17% low
0.208	0.602	0.1065	0.0196	447	6.5% high
0.187	0.631	0.200	0.02	420	
0.197	0.631	0.171	0.0195	427	15% low
0.187	0.641	0.209	0.0183	420	4.5% high

in u than does the error in Z_1; the two errors are also in the opposite direction. The error in $Z_{0.1}$ also produces large errors in the values determined for ϵ_c and θ_s. The value assumed for u (0.02 atm cm) in the first example is low enough that the emissivity at the line center is still near the linear region; i.e., the emissivity is nearly proportional to u. The emissivity is definitely too high to be in the linear region for the larger values of u represented in the table.

Only small values of ϵ_c (0.005) are assumed for the upper portion of the table, which corresponds to low values of Y_{att}. If larger values of ϵ_c had been assumed for the same values of u and Y_{att}, the resulting temperature would have been well below the temperature range of interest. As expected, percentage errors in u are lower for the larger values of u represented in the lower portion of the table.

SECTION VI

EXPERIMENTAL PROCEDURES

OPTICAL APPARATUS

Figure 18 shows a schematic diagram of the optical apparatus used for most of the emission measurements. The emitting gas being studied (called the sample) is contained in a 1.42-cm long sample cell, which consists of a stainless steel body with NaCl windows. Silicone rubber O-rings provide a good vacuum seal between the windows and the cell body. The diameter of the opening through the windows is approximately 1.8 cm. The sample cell is supported inside a piece of ceramic tubing with approximately 7 cm inside diameter. The ceramic tubing forms the core of an electric furnace that is manually controlled to the desired temperature. All samples studied were at 1 atm total pressure. The cell can be evacuated or filled with non-emitting N_2 in order to obtain background data corresponding to no sample gas. Two gas lines connected to the cell make it possible to flush a sample through the cell continuously to avoid errors that might arise from leakage in the lines or from adsorption of some of the sample gas on the walls of the tubing or of the sample cell. When a measurement is being made, the gas flow is either stopped or adjusted low enough so that the gas in the cell has time to reach equilibrium temperature.

The sample can be measured either in emission or in absorption. When measuring the absorption, a Nernst glower serves as a source of radiant energy that is chopped at 450 Hz by chopper 1. The energy beam is directed through the sample cell with an image of the Nernst glower formed near the center of the sample cell. Chopper 2 is stopped in the open position so that another image of the Nernst is formed on aperture Ap 3. From there, the beam travels through the grating assembly to the liquid-nitrogen-cooled InSb detector. (The grating assembly serves as a spectral filter and is discussed in the following subsection.) The detector signal is processed by a synchronous demodulator and amplifier that produces a dc signal that is proportional to the 450 Hz component of the energy incident on the detector. Radiant energy emitted by the sample cell is not chopped and therefore does not produce an output signal. The average transmittance of a sample is measured by comparing the signal output observed with the sample in the cell to that observed with the sample cell evacuated. The ratio of these two signals corresponds to the average transmittance of the sample over the narrow spectral interval passed by the combination grating assembly and filter. The filter placed immediately in front of the detector passes a spectral band that includes the narrow interval transmitted by the grating assembly and blocks higher orders of shorter wavelength energy that are also passed by the grating assembly.

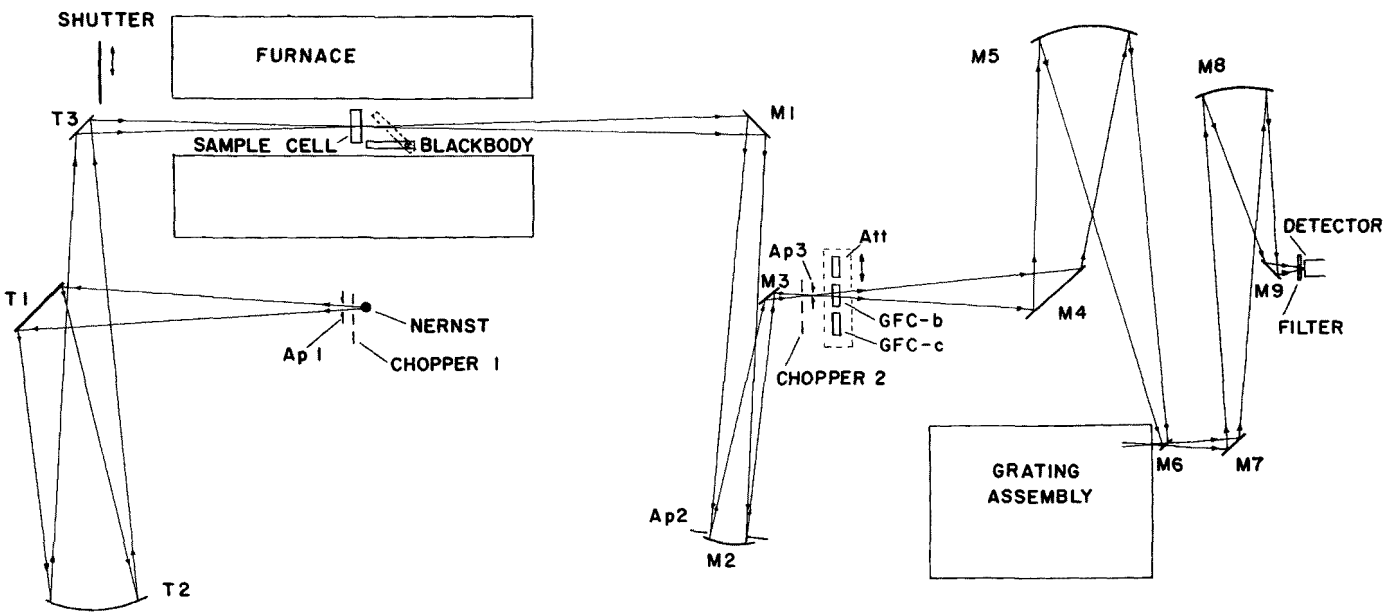

Figure 18. Optical diagram of the apparatus used with a 1.42-cm sample cell.

When the gas is being studied in emission, the shutter near mirror T3 is moved into the beam to block energy from the Nernst. Chopper 1 is turned off and chopper 2, which also operates at 450 Hz, is turned on. The blackened blades of chopper 2 are at room temperature; therefore, the signal output of the synchronous demodulator is proportional to the radiance of the sample cell plus the room-temperature background objects minus the radiance of the black chopper. The spectral radiance of a blackbody at typical sample temperatures in the spectral interval of interest is from 10 to 25 times as much as the spectral radiance of a blackbody at room temperature. Therefore, the signal is nearly proportional to the absolute spectral radiance of the sample cell. The shutter near mirror T3 is also maintained at room temperature so that no signal is produced by background objects when the hot sample cell is removed from the optical path.

Apertures Ap 1, Ap 2, and Ap 3 limit the effective field-of-view. Aperture Ap 1 limits the height of the image formed on the window of the sample cell so that none of the light is blocked by the walls of the cell. This makes it convenient to use the visible light from the Nernst to align all of the optics between the sample cell and the detector and to determine the field-of-view. In aligning the cell, the image formed at the sample cell is reimaged on a small aperture, Ap 3, which is slightly smaller than the image formed on it. Aperture Ap 3 is then imaged on the entrance slit of the grating assembly. Both dimensions of the slit are smaller than the corresponding dimensions of the image formed, so that the slit is completely illuminated and the amount of signal is not subject to slight movement of the image on the slit. Aperture Ap 3 is not required to limit the size of the image, but it is useful in reducing the amount of modulated energy reaching the detector from the blades of the rotating chopper 2. Aperture Ap 2 is sufficiently small that it determines the angular divergence of the beam that reaches the detector. All of the succeeding mirrors and components in the grating assembly, with the exception of the slit,which is at an image, are underfilled. The sensitive area of the detector is larger than the image of the exit slit formed on it. Therefore, the field-of-view is limited by the entrance slit of the grating assembly and aperture Ap 2. No energy emitted by the core of the furnace, except for a very small amount that is scattered by the windows of the sample cell, can reach the detector. Light shields not shown in the figure limit the stray radiant energy.

The component labeled as a blackbody in the furnace is a piece of black-anodized aluminum that can be remotely moved into or out of the path from which energy can reach the detector. This blackbody is at nearly the same temperature as the sample and provides a continuous source of radiant energy over the spectral interval of interest so that the average transmittances of attenuators and GFC's can be balanced as suggested in Section V. Although the emissivity of this blackbody is somewhat less than unity, the energy reaching the detector from its surface is essentially that of a blackbody at its temperature because any energy reflected by the surface originated from the inside surface of the furnace core. The core is also at nearly the same temperature as the sample cell. Small errors in the effective spectral radiance of the blackbody do not cause any significant problem in the reduction of the data. A polished sapphire window placed adjacent to the sample cell for a few measurements simulated continuum emission with emissivity of 0.06.

The assembly that contains the attenuator (Att) and the two gas-filter cells (GFC-b and GFC-c) corresponds to the alternator in Figure 1. The attenautor and the two GFC's are mounted on a single assembly that can be moved manually so that either of the three components, or none of them, is in position for the energy beam to pass through it. The sliding assembly has a guide and stops so that the positions of the components in the beam can be reproduced accurately. Each GFC is one cm long with an effective diameter of approximately 2 cm. GFC-b is filled with pure NO to 1 atm pressure; GFC-c is also filled with pure NO, but to a total pressure of only 0.1 atm. The corresponding absorber thicknesses, w, for cells GFC-b and GFC-c are 1.0 and 0.1 atm cm, respectively. The GFC's and the attenuator are at room temperature. The attenuator consists of two sapphire windows that are similar to the ones on the GFC's. Both surfaces of each window are anti-reflection coated to increase the amount of transmitted energy and to avoid potentially troublesome "fringes" that can result from interference between the energy reflected from the two surfaces of each window.

As discussed in Section V, a field instrument operating on the principles of the instrument used for these laboratory tests would probably contain an alternator that rapidly moves either one of the GFC's or the attenuator into the beam at a frequency between 1 Hz and 30 Hz. The detector signal would then be processed in such a way as to accurately measure the small differences between the amounts of energy passing through each of the three components. Furthermore, each of the GFC's would have associated with it a neutral-density attenuator so that the three components on the alternator would be optically balanced when the source of radiant energy was a blackbody near the temperature of the samples to be studied. This means that the amount of radiant energy passing through each of the three components would be the same. Of course, the addition of hot NO to the sample would cause a misbalance in the attenuator because of the selective absorption characteristics of the NO in the GFC's.

In the laboratory instrument illustrated in Figure 18, it was not necessary to incorporate the accurately adjusted attenuators in series with the GFC's. The signal passing through each GFC, or the attenuator, was measured by manually sliding the assembly until the appropriate component was in the energy beam; the average of the signal output as displayed on the strip chart recorder was measured over a period of 10 to 30 seconds. An appropriate "correction factor" was determined for each of the components to account for the differences between the output signals observed through each of the components when the blackbody was being used. The appropriate correction factors were then applied to the output signal observed when an NO sample was being investigated.

Typically, the minimum detectable difference between two signals observed through a GFC and an attenuator was approximately 0.2%. Smaller fractional differences could, of course, be observed if the components of the alternator were moved into and out of the beam rapidly and the small differences were measured directly. This smaller fractional difference in the minimum detectable observed signal would correspond to smaller minimum detectable concentrations of NO. The method used here in the laboratory instrument was easier to incorporate and was adequate for the purposes of the investigation because the fractional modulation of smaller samples can be determined by extrapolating from the data obtained.

The receiver portion of the apparatus shown in Figure 19 is the same as the corresponding portion of the instrument in Figure 18. The sample cell illustrated in Figure 19 has a base length of 1 meter and uses a mirror inside of the sample cell to produce an optical path-length of 2 meters. The arrangement illustrated in Figure 19 was used to obtain some additional data on samples of NO, but it was used primarily to investigate the interference by emission by hot H_2O. All of the H_2O data were obtained with samples near 440 K; all samples were at a total pressure of 1 atm and were introduced into the sample cell through gas lines that were heated to avoid condensation. Mixtures of H_2O + N_2 were made by first introducing the H_2O into the cell to the desired pressure; the valve at the cell was then closed and the lines were evacuated. The N_2 was then added to approximately 1 atm pressure. The sample cell was evacuated to obtain background data corresponding to no NO or H_2O in the sample. The optical path through the atmosphere is approximately 8 m long and typically contained approximately 40% relative humidity at 296 K.

The double-pass sample cell has an inside diameter of approximately 10 cm and is wrapped with heating wire and insulation capable of maintaining a constant and uniform temperature up to approximately 470 K. The box that contains part of the insulation extends beyond the cell to minimize cooling of the end of the cell on which the windows are mounted. Five thermocouples mounted at different positions on the cell and on one of the windows are used to monitor the temperature at the various points. The temperatures are typically the same to within $\pm$ 3°C. The emissivities of the two windows and the mirror MC in the sample cell are such that the energy received from the evacuated cell corresponds to a gray-body with approximately 8% emissivity at the temperature of the cell. This relatively small amount of emission can be accounted for in order to determine the signals that would be observed with isolated gas samples corresponding to ones in the sample cells. Mirror MC and the windows of the sample cell are sufficiently over-sized that the field-of-view is determined by the entrance slit of the grating assembly and aperture Ap 2. As with the apparatus illustrated in Figure 18, the gas sample can be studied in absorption by stopping chopper 2 in the open position and turning on chopper 1 and the Nernst source. The shutter near mirror T1 is moved into the beam during emission studies and is out of the beam during absorption studies.

SELECTION OF SPECTRAL INTERVAL

Nitric oxide is a diatomic molecule and therefore has only one strong, fundamental vibration-rotation absorption band in the infrared. Thus, any remote sensing system involving infrared energy must make use of this band, which is centered near 1876 cm^{-1}. The band contains many strong, well-separated absorption lines, making it a good candidate for gas-filter correlation techniques. Undoubtedly, the most difficult problem involved in the remote sensing of NO by GFC techniques results from interference by H_2O, which also absorbs and emits throughout a spectral region that includes the NO band. The proper selection of the spectral interval is very important, more because of the need to reduce the possible interference by H_2O than to optimize the sensitivity of the instrument. In previous investigations, we have found that interference by H_2O cannot be completely avoided, but it can be greatly reduced by careful

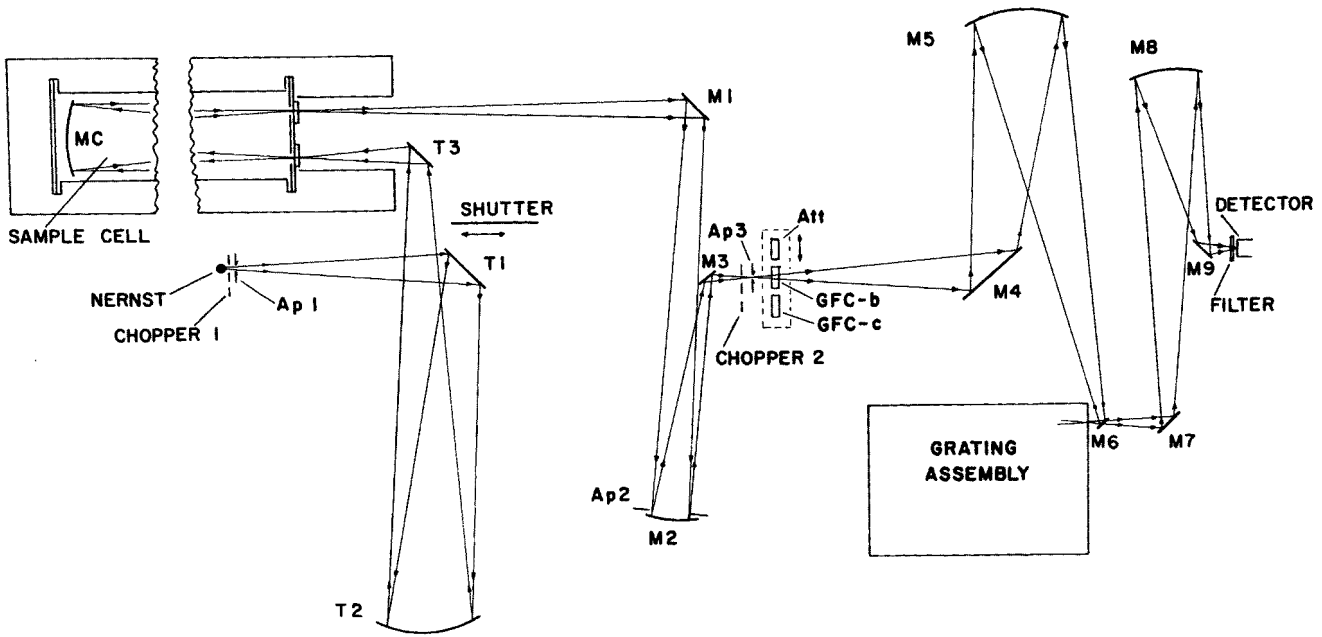

Figure 19. Optical diagram of the apparatus used with a 200-cm sample cell.

selection of the narrow spectral interval, or intervals, to be used. It is apparent that the spectral interval must be sufficiently narrow and positioned so as to include a minimum of H_2O lines and not include excessive continuum emission or absorption by the extreme wings of strong H_2O lines centered outside of the interval. The minimum practical width of the interval is limited by the minimum amount of energy that must be received in order that the observed signals are large compared to the detector noise.

Figure 20 shows transmission spectra of NO and H_2O over the region that contains most of the R-branch of the NO band. The need for care in minimizing the interference by H_2O is apparent from the amount of absorption and emission by H_2O. The absorption by H_2O is even stronger in the P-branch of the NO band, which occurs at lower wavenumbers than those included in the figure.

An optical arrangement similar to that shown in Figure 19 was employed to obtain the data illustrated in Figure 20. The Nernst glower was used along with chopper 1, making it possible to measure the transmittance of samples contained in either the heated 200-cm sample cell or in one of the GFC's. The beam of radiant energy was intercepted by a mirror placed just ahead of mirror M6 (Figure 19) to divert the beam to a small grating monochromator that is not shown in the figure. Panel III of Figure 20 shows the spectrum of the H_2O in the approximately 8-meter air path of the energy beam. Panels I and II contain spectra of NO in addition to the H_2O in the air path. Most of the structure in the spectra due to NO can be observed by comparing either Panel I or II with Panel III to account for the H_2O absorption. The 445 K sample represented in Panel I consists of a 1 atm mixture of 0.1% NO in N_2 in the 200-cm cell. The 296 K sample represented in Panel II consists of a 1 atm mixture of 20% NO in N_2 in one of the 1-cm long GFC's.

The influence of increased temperature on the absorption characteristics of NO can be seen by carefully comparing a few of the NO absorption lines in Panels I and II. For example, the pair of barely resolved lines very near 1900 cm^{-1} absorb more in the 296 K sample than in the higher-temperature sample. The relative amounts of absorption are reversed for the higher wavenumber lines in the H_2O vapor window between approximately 1924 and 1940 cm^{-1}. Near 1900 cm^{-1}, the absorption is greater by the low-temperature sample because it contains more NO molecules per unit cross-section of the energy beam. In addition, the intensities of the NO lines in this spectral region are slightly lower at the higher temperature than at 296 K. On the other hand, the increase in the populations of the energy levels involved in the transitions that produce the higher wavenumber lines cause the intensities of these lines to increase rapidly with increasing temperature.

Panel IV of Figure 20 shows three spectra of H_2O and $H_2O + N_2$ mixtures at 445 K in the 200-cm cell. The mixtures of 10% H_2O and of 30% H_2O are at a total pressure of 1 atm. The 100% H_2O mixture is at approximately 0.95 atm. These three spectra of hot H_2O illustrate the spectral features of typical absorber thicknesses of H_2O that might be present in the exhaust from stacks of interest. Interference in the measurement of NO by H_2O samples similar to those represented in Panel IV has been investigated and is discussed in Section VII.

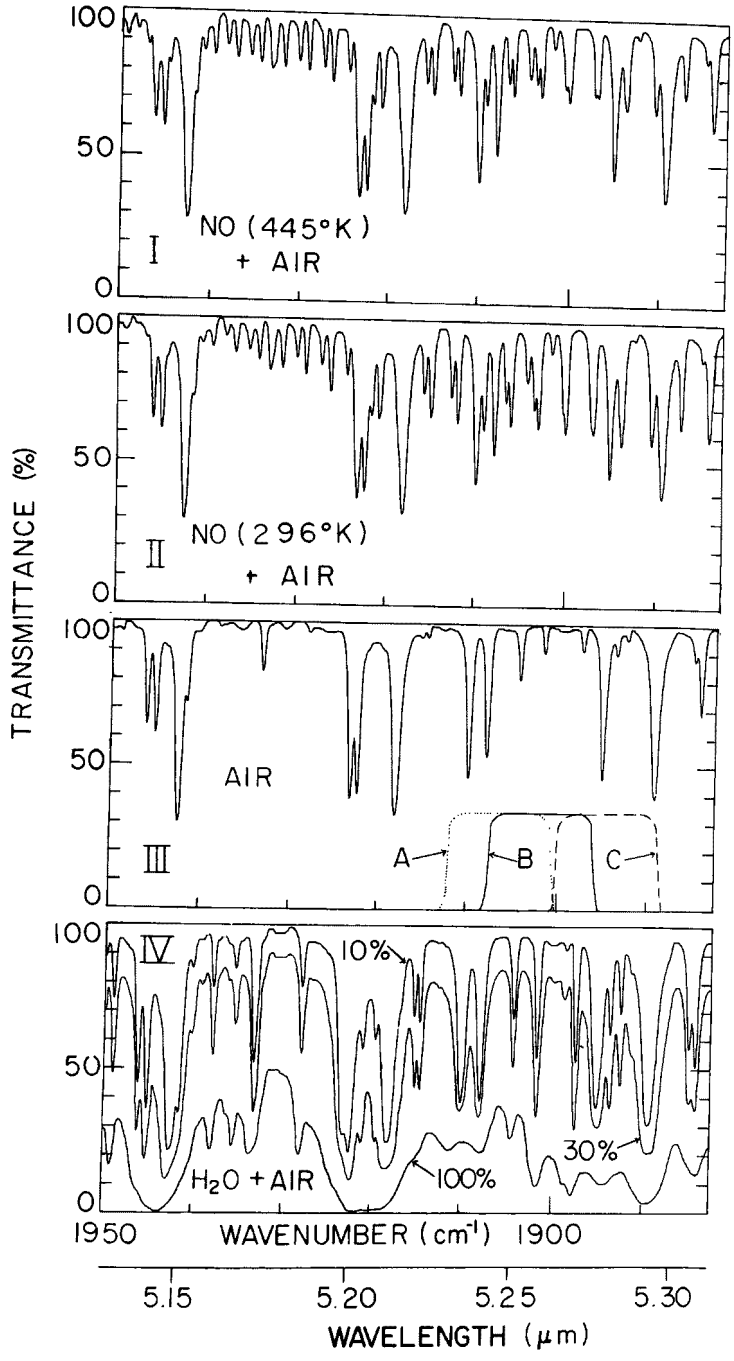

Figure 20. Transmission spectra of H_2O and NO and of the bandpass of the grating assembly. The H_2O in the 8-meter air path contributes to the absorption observed for all of the samples. The precentages of H_2O in the $H_2O + N_2$ mixtures represented by Panel IV are indicated.

Curves A, B, and C in Panel III of Figure 20 illustrate the three spectral bandpasses employed. The transmittance scale for these three curves is in arbitrary units. The shapes and positions of the curves were determined by passing a beam of energy through the grating assembly to a grating monochromator that was used to scan the spectra. All of the data, except for some of the data on H_2O interference, presented in Section VII were obtained while using the spectral interval corresponding to Curve B. This interval was selected to include a minimum of H_2O absorption while containing four pairs of strong NO lines. The lines passed correspond to 2 m = 13, 15, 17, and 19. A pair of adjacent lines exist for each of these four values of 2 m. One line of each pair corresponds to the subband of $\Omega = + 1/2$; the other corresponds to $\Omega = 3/2$. The higher wavenumbers correspond to the large values of 2 m. The spectral slitwidth used in obtaining the spectra of Figure 20 was narrow enough that the pairs of lines corresponding to 2 m = 17 and 19 are barely resolved; whereas those corresponding to 2 m = 13 and 15 are not resolved. The positions, intensities, and half-widths of the NO lines have been reported by a number of workers, including Shaw[2] and Abels and Shaw[3].

The selection of the spectral interval is based on the previous studies carried out in our laboratory[1,4]. It represents an optimization of minimum interference by H_2O, sensitivity to NO, energy throughput, and the possibility of matching it with an interference filter. A small, fixed-position grating assembly is used in the present instrument to produce the accurately defined spectral interval. The grating assembly is similar to those described in previous reports by us[1,4] and has the important advantage that the spectral interval can be carefully tailored during the course of the experiment. A grating assembly of this type would probably not be used in a field instrument because of its complexity and because of the relatively small energy throughput to which it is limited. However, it is likely that a small interference filter could be designed and built to pass a spectral interval very close to the one passed by the laboratory instrument. The energy throughput of an instrument using such an interference filter could be several times as great as that of the laboratory instrument, making it possible to investigate more distant sources, or smaller sources, than could be investigated with the laboratory instrument.

Near the end of the measurements, one of the mirrors in the grating assembly was readjusted to shift the spectral interval to either of the two positions indicated by curves A and C in the Panel III of Figure 20. A few measurements were made at each of these latter two intervals in order to investigate the effect of shifting or widening the spectral interval so that it contains more of the strong H_2O absorption.

---

2. Shaw, J. H. Nitric Oxide Fundamental. J. Chem. Phys. 24:399-402, 1956.

3. Abels, L. L. and J. H. Shaw. Width and Strengths of Vibration-Rotation Lines in the Fundamental Band of Nitric Oxide. Journ. Molecular Spectroscopy 20:11-28, 1966.

4. Gryvnak, D. A. and D. E. Burch. Monitoring NO and CO in Aircraft Jet Exhaust by a Gas-Filter Correlation Technique. AFAPL-TR-75-101, Air Force Wright Aeronautical Laboratories, Wright-Patterson Air Force Base, Ohio. Prepared by Aeronutronic Ford Corp., under Contract No. F33615-75-C-2038, Jan. 1976.

RADIOMETRIC CALIBRATION AND CORRECTION FOR CHOPPER EMISSION

The radiant power reaching the detector from the sample when the chopper is in the open position and there is no attenuator or GFC in the beam is given by

$$E = M \int N_\nu^B \, \epsilon_s \, d\nu \tag{9}$$

(see Equation (7)). The integration covers the spectral interval passed by the grating assembly, and M is a constant for a given optical apparatus. When the attenuator is moved into the beam, the incident power is reduced by a factor equal to T_{att}, the transmittance of the attenuator. Thus

$$E_{att} = M \, T_{att} \int N_\nu^B \, \epsilon_s \, d\nu \, . \tag{10}$$

The detector signal is processed by a synchronous demodulator, making the effective detector signal, D_{att}, proportional to the difference between the power levels incident on the detector during the two halves of the chopper cycle indicated by (open) and (closed). The responsivity R of the detector is defined by

$$D_{att} = R \left[E_{att} \text{ (open)} - E_{att} \text{ (closed)} \right] . \tag{11}$$

Calibration of the instrument is complicated by the emission by the chopper blade, which can be assumed to be a blackbody at room temperature (296 K), and by the room-temperature walls of the laboratory. We are concerned only with radiant energy from paths that change from one half of the chopper cycle to the other. Energy emitted by components between the chopper and the detector is not chopped; therefore it is not detected. When the chopper is open

$$E_{att} \text{ (open)} = M \, T_{att} \left[\int N_\nu^B \text{ (sample temp.)} \, \epsilon_s \, d\nu + \int N_\nu^B \text{ (296 K)} (1-\epsilon_s) \, d\nu \right] . \tag{12}$$

N_ν^B (sample temp.) and N_ν^B (296 K) represent the spectral radiances of blackbodies at the sample temperature and at 296 K, respectively. The transmittance, T_s, of the sample is equal to $(1 - \epsilon_s)$. The first term in the equation corresponds to the power emitted by the sample through the attenuator and other optical components to the detector. The second term represents the power emitted by the wall, or by other room-temperature objects, that passes through the sample cell to the detector. The corresponding equation for E_{att} (closed) gives the power emitted by the chopper blade,

$$E_{att} \text{ (closed)} = M \, T_{att} \int N_\nu^B \text{ (296 K)} \, d\nu. \tag{13}$$

Combining Equations (11), (12), and (13) gives

$$D_{att} = RM \, T_{att} \left[N_\nu^B \text{ (sample temp.)} - N_\nu^B \text{(296 K)} \right] \int \epsilon_s \, d\nu. \tag{14}$$

The values of N_ν^B are calculated, and T_{att} is measured. The spectral bandpass can be approximated by an 11 cm^{-1} interval of constant transmittance. By measuring D_{att} for a sample of known average emissivity $\bar{\epsilon}_s$, the product of the two constants R and M is determined. It is not necessary to determine the values of R and M individually; as long as their product, RM, is known, the detector signals can be related directly to values of Y_j (see Equation (7)).

Values of blackbody spectral radiance are listed in Table 2 for several temperatures of interest. The values at 1901 cm^{-1} correspond closely to the center of the spectral band passed by the grating assembly. The ends of the interval are near 1896 cm^{-1} and 1906 cm^{-1}, the other two wavenumbers for which the spectral radiance is tabulated. The ratio of the radiances near the end-points indicates the slight change in the slope of the spectral radiance curve as the temperature changes. Because N_ν^B for any typical stack temperature is nearly constant over the effective spectral interval, the values of the quantities in Equations (12) and (13) are changed very little by removing N_ν^B from under the integral sign and using the mean value of this quantity for a fixed temperature as a constant factor.

The radiometric calibration was performed by using the known average emissivity of the 100% NO samples at 1 atm. The average absorptance, which is equivalent to the average emissivity, was measured by using chopper 1 with the Nernst glower source. By comparing the detector signal observed with the sample cell evacuated to that observed with it filled with gas, the average absorptance was measured quite accurately. At the four temperatures of interest, the average absorptances (emissivity) for the 1 atm sample in the 1.42-cm cell are: 406 K, 0.364; 423 K, 0.352; 431 K, 0.347; 450 K, 0.337. The appropriate value of average emissivity was used in Equation (14) to determine the value of the product RM. It was necessary to adjust the values of D_{att} slightly to account for the small amount of energy emitted by the cell windows. The method used to account for the window emission is discussed in the next sub-section of this report.

Errors in the value used for RM do not change the values determined for Z_1 and $Z_{0.1}$ (see Equation (8)) as long as the instrument is stable and the same value of RM is used for all data in one set. One set consists of all of the values of detector signal observed through each GFC and the attenuator for all of the different gas concentrations at a single temperature. The accuracy of the value of Y_{att} attributed to a given sample is, of course, directly dependent on the accuracy with which RM is determined.

We had originally intended to use the block of black-anodized aluminum mounted on a hinge near the 1.42-cm sample cell as a blackbody ($\epsilon_s = 1$) of known temperature to determine RM. However, during the tests we found that the surface of the aluminum block apparently had a significant reflectivity. This allowed a small amount of energy emitted by the core of the furnace to be scattered into the beam received by the detector. Because of a difference between the temperatures of the anodized aluminum block and the furnace core, the energy emitted by the core changed the effective radiance temperature. In addition, the temperature of the aluminum block varied after it was raised into the beam received by the detector. The uncertainty in the effective radiation temperature of the aluminum block made it unsatisfactory as a means of determining

TABLE 2

SPECTRAL RADIANCE OF A BLACKBODY FOR TEMPERATURES AND WAVENUMBERS OF INTEREST

Temp. (K)	$N_\nu^B \left(\frac{\mu watts}{cm^2\ cm^{-1}\ ster}\right)$ $\nu\ (cm^{-1})$ 1896	1901	1906	$\frac{N_\nu^B\ (1906\ cm^{-1})}{N_\nu^B\ (1896\ cm^{-1})}$
296	0.8070	0.7944	0.7819	0.9689
390	7.447	7.372	7.297	0.9799
400	8.871	8.786	8.701	0.9808
410	10.48	10.38	10.29	0.9819
420	12.28	12.17	12.06	0.9821
430	14.29	14.17	14.05	0.9832
440	16.51	16.37	16.24	0.9837
450	18.95	18.81	18.66	0.9847
460	21.63	21.47	21.31	0.9852
2000	2788.	2797.	2805.	1.0063

the constant that related output signal to source radiance. This block was adequate, however, as a continuous energy source near the sample temperature to determine the relative average transmittances of the attenuator and the two GFC's.

As is evident from the theoretical data of Section V, the accuracy of a field instrument of the type considered here depends strongly on the ability to measure accurately a small difference between two power levels. The ratio Z_j (Equation (8)) is proportional to the difference between the radiant power transmited through two different optical components, the attenuator and a GFC. The instrument is designed so that this difference is to be adjusted to zero when the source of radiant energy is a blackbody at the same temperature as the sample gas. This adjustment is referred to as balancing the alternator and amounts to "zeroing" the instrument. (The alternator consists of the attenuator and the GFC's.) The temperature of the gas in the effluent from a stack is ordinarily not known; therefore, it is important to know how strongly the balance of the attenuator depends on the temperature of the blackbody used as the energy source.

With this problem in mind, we carefully measured the effective average transmittance of the two GFC's with continuous energy sources at three different temperatures. One of the sources was the black-anodized aluminum block labeled as a blackbody in Figure 18. This source was at approximately 450 K. The optical apparatus illustrated in Figure 18 was employed, and the average transmittance was determined by measuring the detector signal with the GFC evacuated and with it filled with pure NO. One cell was filled with 0.1 atm of NO and the other with 1 atm. The same gas-sampling procedure was followed while using the Nernst glower as a source. One set of measurements was made with the Nernst glower operating at approximately 2300 K; another set was made with the current adjusted much lower so that the Nernst was only at about 1300 K. No significant difference was observed in the average transmittance for the same amount of NO. A difference as small as $\pm$ 0.002 in transmittance would have probably been observable.

The right-hand column of Table 2 indicates that the slope of the spectral radiance curves would be different for the three different temperatures. Thus, the very slight dependence, if there is any dependence at all, of the average transmittance on source temperature indicates that the NO transmittance is approximately symmetrical within the spectral bandpass. For example, if most of the NO absorption occurred on the high-wavenumber side of the interval, the average transmittance would be expected to decrease with increasing temperature. The results indicate that the alternator balance would be very insensitive to changes in source temperature. Therefore, no significant error in the laboratory measurements are expected to result because of the slight difference between the temperatures of the sample gas and the blackbody used to balance the attenuator.

CORRECTION FOR WINDOW EMISSION

By comparing the radiance of the evacuated 1.42-cm sample cell to the radiance of the sample cell filled with 1 atm of pure NO, we determined that the effective emissivity of the cell windows was approximately 0.03. This effective emissivity is higher than was expected; the bulk emissivity of NaCl is known

to be very low at the wavenumbers (near 1900 cm^{-1}) and temperatures (390 - 460 K) of interest. The observed apparent emissivity of the windows has been attributed to scattering by the surfaces of the windows, which were slightly "foggy" because of previous contact with humid air. A small amount of energy emitted by the inside wall of the furnace core apparently was scattered by the window surfaces into the beam of energy received by the detector. It is not necessary that the continuum emission by the windows be known accurately, or that its origin be completely understood, in order to account for it adequately in determining the contribution to the emission by the hot NO.

If the emitting NO and the windows that produce the continuum emission are at the same temperature, the emissivity ϵ (gas + window continuum) for the combination is related to the separate emissivities by

$$\epsilon\ (\text{gas + window continuum}) = \epsilon\ (\text{gas}) + \epsilon\ (\text{window continuum}) - \epsilon\ (\text{gas}) \cdot \epsilon\ (\text{window continuum}). \quad (15)$$

From this expression it follows that the value of Y_j (gas only) that would be observed for the gas only is given by

$$Y_j\ (\text{gas only}) = \frac{Y_j\ (\text{gas + window continuum}) - Y_j\ (\text{window continuum})}{1 - \epsilon_c\ (\text{window continuum})}. \quad (16)$$

The numerator represents the difference in Y_j produced by adding the NO + N_2 gas mixture to the sample cell. The denominator $\cong 1 - 0.03 = 0.97$. It is apparent that a small error in ϵ (window continuum) will not cause a sizeable error in the corrected value of Y_j (gas only). The accuracy of Y_j (gas only) for mixtures of low NO concentration depends strongly on the accuracy with which the small difference corresponding to the numerator of Equation (16) can be measured. Equation (16) was used in reducing the emission data to determine values of Y_{att}, Y_1, and $Y_{0.1}$ that correspond to the gas in the sample cell.

DETERMINATION OF CORRELATION FROM TRANSMITTANCES

The apparent radiance of a source of hot NO depends on whether it is viewed through an attenuator or through a GFC containing NO. The differences in the apparent radiance result from the strong correlation between the spectral structures of the hot emitting gas and the gas in the GFC. By making a few simple assumptions that are essentially valid for the instrument described here, this correlation can, at least in principle, be determined from a series of transmission measurements. Values of Z_j that would be determined by emission measurements can therefore be calculated from the results of the transmission measurements. The more accurate of the two methods depends on a combination of several parameters, including sample temperature and sample emissivity.

The mathematical equivalence of the two methods is illustrated by the derivations and suggested measurements given below. It is assumed that the following

three quantities are essentially constant over the narrow spectral interval passed by the instrument: N_ν^B, the spectral radiance of a blackbody at either the temperature of the sample or of the Nernst glower used as an energy source for the transmission measurements; ϵ(Nernst), the emissivity of the Nernst glower; and T_{att}, the transmittance of the attenuator. Recall that $T_s = 1 - \epsilon_s$, and that the instrument is balanced so that $\int T_1 \, d\nu = \int T_{0.1} \, d\nu = \int T_{att} \, d\nu$.

Consider the situation in which the Nernst glower and chopper 1 are being used to measure sample transmittances. The detector signal observed with no gas in the sample cell and with the attenuator in the beam is given by

$$D^o(att) = (\text{Constant}) \, N_\nu^B \, \epsilon(\text{Nernst}) \int T_{att} \, d\nu. \tag{17}$$

$N_\nu^B \, \epsilon$(Nernst) is much greater than the corresponding quantity for the chopper, which can therefore be ignored. When a sample of transmittance T_s is added, the detector signal is reduced to

$$D(att) = (\text{Constant}) \, N_\nu^B \, \epsilon(\text{Nernst}) \int T_s \, T_{att} \, d\nu. \tag{18}$$

The ratio, D/D^o, of these two quantities is determined by measuring the detector signals with the sample cell empty and with the sample gas in the cell,

$$\frac{D(att)}{D^o(att)} = \frac{\int T_s \, T_{att} \, d\nu}{\int T_{att} \, d\nu} = \frac{\overline{T_s \, T_{att}}}{\overline{T}_{att}} = \overline{T}_s \, . \tag{19}$$

The corresponding ratios are measured, first with GFC-b, then with GFC-c replacing the attenuator. These two GFC's contain w = 1 atm cm and 0.1 atm cm, respectively. From these two measurements, we obtain

$$\frac{D(w = 1)}{D^o(w = 1)} = \frac{\overline{T_s \, T_1}}{\overline{T}_1} \, , \text{ and} \tag{20}$$

$$\frac{D(w = 0.1)}{D^o(w = 0.1)} = \frac{\overline{T_s \, T_{0.1}}}{\overline{T}_{0.1}} \, . \tag{21}$$

The expression given by Equation (19) reduces to $\overline{T}_s$ because $T_{att} = \overline{T}_{att}$ is constant. However, a similar simplification can not be made to Equations (20) and (21) because neither T_s, T_1, nor $T_{0.1}$ is constant.

We now consider the emission measurements of Y_{att}, Y_1 and $Y_{0.1}$, made for the same sample by the methods described previously in this report. In this case N_ν^B refers to the spectral radiance of a blackbody at the temperature of the sample, and ϵ_s is written as $1 - T_s$.

$$Y_{att} = N_\nu^B \left[\int T_{att}\, d\nu - \int T_s\, T_{att}\, d\nu \right] , \tag{22}$$

$$Y_1 = N_\nu^B \left[\int T_1\, d\nu - \int T_s\, T_1\, d\nu \right] , \text{ and} \tag{23}$$

$$Y_{0.1} = N_\nu^B \left[\int T_{0.1}\, d\nu - \int T_s\, T_{0.1}\, d\nu \right] . \tag{24}$$

Combining the latter three equations to give Z_1 and $Z_{0.1}$ as defined by Equation (8) yields

$$Z_1 = \frac{1}{(1 - \overline{T}_s)} \left[\frac{\overline{T_s\, T_1}}{\overline{T}_1} - \overline{T}_s \right] , \text{ and} \tag{25}$$

$$Z_{0.1} = \frac{1}{(1 - \overline{T}_s)} \left[\frac{\overline{T_s\, T_{0.1}}}{\overline{T}_{0.1}} - \overline{T}_s \right] . \tag{26}$$

Note that the quantities in Equations (25) and (26) are the ones determined by the suggested transmission measurements. Values of Z_1 and $Z_{0.1}$ have been determined by both methods, emission and transmission, for many of the samples to provide a check of consistency. Generally, the results obtained by the two methods agree quite well. All of the data shown in Section VII for samples of NO, or of NO with continuum, are based on emission measurements. Data obtained by both methods are presented for samples containing H_2O.

SECTION VII

RESULTS OF LABORATORY MEASUREMENTS

RADIANCE OF NO SAMPLES

The average absorptance was measured for samples with the same parameters as those to be studied in emission. All of the samples consisted of NO + N_2 mixtures contained in the 1.42-cm long sample cell at a total pressure of 1 atm. The NO concentrations for the various mixtures were: 1%, 2.5%, 5%, 10%, 20%, 40% and 100%. Figure 21 shows logarithmic plots of the average absorptance, $\bar{A}_g$, of the different mixtures as a function of the sample absorber thickness u. The two temperatures, 410 K and 450 K, represent the lowest and highest temperatures at which emission data were obtained. Data points corresponding to intermediate temperatures were not plotted in order to avoid crowding, but they would fall, as expected, between the two curves shown.

Chopper 1 interrupted the beam of energy from the Nernst glower before it entered the sample cell so that the detector did not respond to energy emitted by the sample cell. The average absorptance was determined by comparing the detector signal observed while the sample was in the sample cell to the signal observed with the cell evacuated. The quantity measured corresponds to the average absorptance over the spectral interval indicated by curve B in panel III of Figure 20. This same spectral bandpass was employed for all of the absorption and emission data described in this section with the exception of a few H_2O interference data discussed below.

As discussed in the previous section, the average absorptance of an NO sample measured over this narrow spectral interval is essentially independent of the temperature of the continuous source used. This is true because the spectral interval is so narrow that the spectral radiance of the blackbody is nearly constant over the entire interval. Because of this, the average absorptance, $\bar{A}_g$, is very nearly equal to the average emissivity, $\bar{\epsilon}_g$, of the same gas mixture. Thus, a logarithmic plot of sample radiance vs u produces a curve with essentially the same shape as the curves shown in Figure 21. The average absorptance, $\bar{A}_g$, and thus $\bar{\epsilon}_g$, of small samples can be measured more accurately in absorption than in emission because the emission by the windows of the sample cell is automatically accounted for by the "sample in-sample out" method used in the absorption measurement. In addition, the spectral radiance of the Nernst glower is many times higher than that of a blackbody near the sample temperature. Therefore, the detector signal observed in absorption is larger and can be measured more accurately. Detector noise limits the accuracy to which small detector signals can be measured.

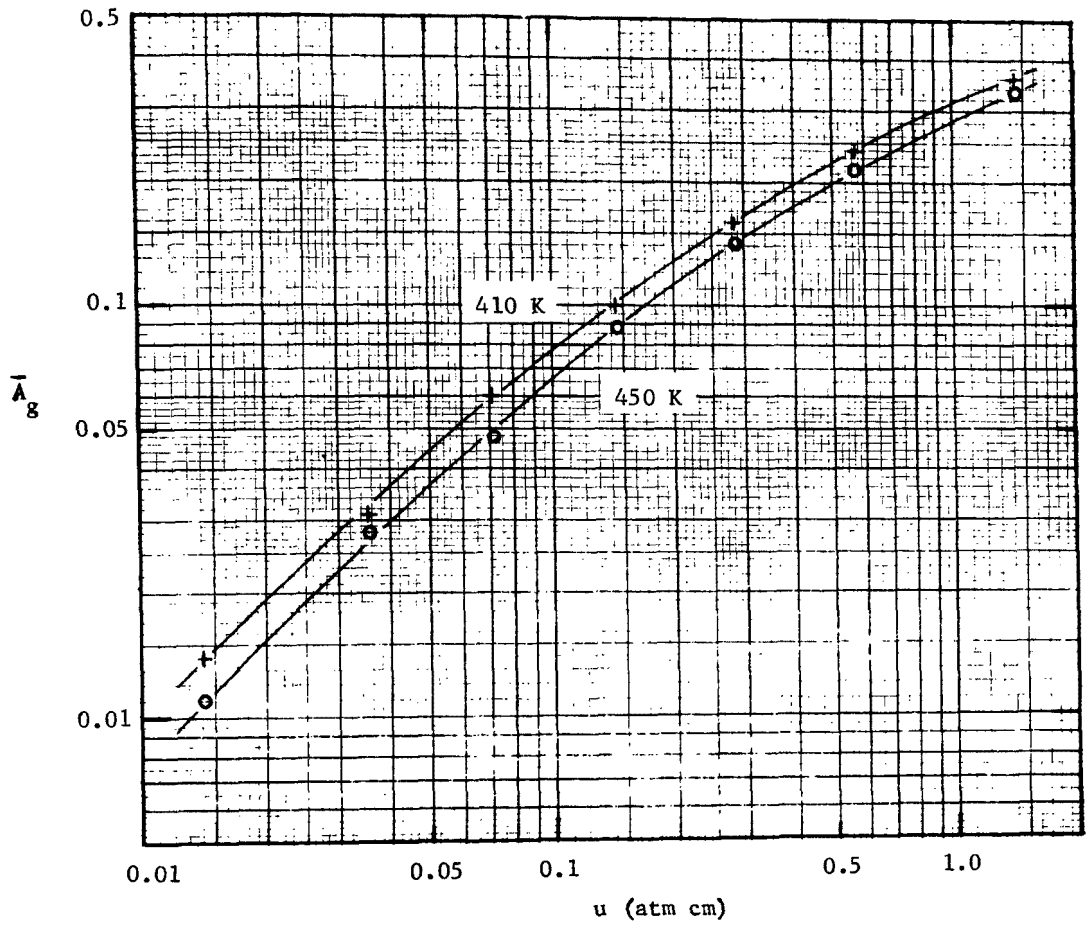

Figure 21. Logarithmic plots of the average absorptance of NO + N_2 mixtures vs u for two temperatures. Sample cell length, 1.42 cm.

When u is less than approximately 0.06 atm cm, the slopes of the curves in Figure 21 are approximately equal to unity. This indicates a near-linear relationship between the absorber thickness and $\bar{A}_g$. For values of u greater than approximately 0.06 atm cm, the individual absorption lines in the sample are nearly opaque near the line centers. As the absorber thickness increases, the only increase in the average absorptance is due to increasing absorption between the lines.

Because of the temperature difference of the two sets of samples represented in Figure 21, a 450 K sample contains approximately 10% fewer molecules/cm^2 than a 410 K sample with the same value of u. By carefully comparing the two curves, we can see that the value of u in the 450 K sample must be approximately 20% greater than the corresponding value to produce the same $\bar{A}_g$ in the 410 K sample. Thus, approximately 10% more molecules/cm^2 are required to produce the same $\bar{A}_g$ at the higher temperature as at the lower temperature. As the temperature of the sample increases, the relative populations of the different vibration-rotation energy levels change in such a way as to reduce the intensities of the lines of NO that occur within the spectral interval passed by the grating assembly. This decrease in the line intensities, along with a slight decrease in the line widths, accounts for the decrease in the absorption cross-section of each molecule as the temperature increases.

EMISSION BY GAS SAMPLES WITHOUT CONTINUUM

The logarithmic plots of Y_i shown in Figure 22 represent the emission data obtained for gas samples at 450 K. The raw data have been adjusted by the procedure discussed in the previous section to account for the continuum emission by the windows of the sample cell. The data represented by the figure corresponds to isolated samples of NO + N_2.

The curve labeled Y_{att} represents the apparent radiance of the samples as they are viewed through the attenuator. The radiance of the samples can be determined by dividing a value from the curve by 0.594, the transmittance T_{att} of the attenuator. The average emissivity of the 1.42 atm cm sample of pure NO at 450 K was previously determined from absorption measurements to be equal to 0.330. This known value of emissivity for this sample was then used by the procedure described in the previous section to determine the constant that relates detector signal to sample radiance. This constant, which is the product RM, (Equation (14)) was then used to relate the detector signal to radiance for all of the other samples represented in Figure 22.

The curve labeled Y_1 represents the apparent radiance of the source as it is viewed through the GFC that contains 1 atm cm of pure NO. Recall from the previous discussions that the detector signals have been adjusted so that $Y_1 = Y_{att}$ when the source of energy is continuous. Approximately 80% of the energy emitted by the samples with u less than 0.04 atm cm is absorbed by the NO in the GFC with w = 1 atm cm. This efficient absorption occurs becuase the gas in the GFC absorbs very strongly at exactly the same wavenumbers where the hot NO in the sample cell emits.

The $Y_{0.1}$ curve corresponds to the energy transmitted through the GFC with 0.1 atm cm of NO. As expected, this curve lies between the other two curves.

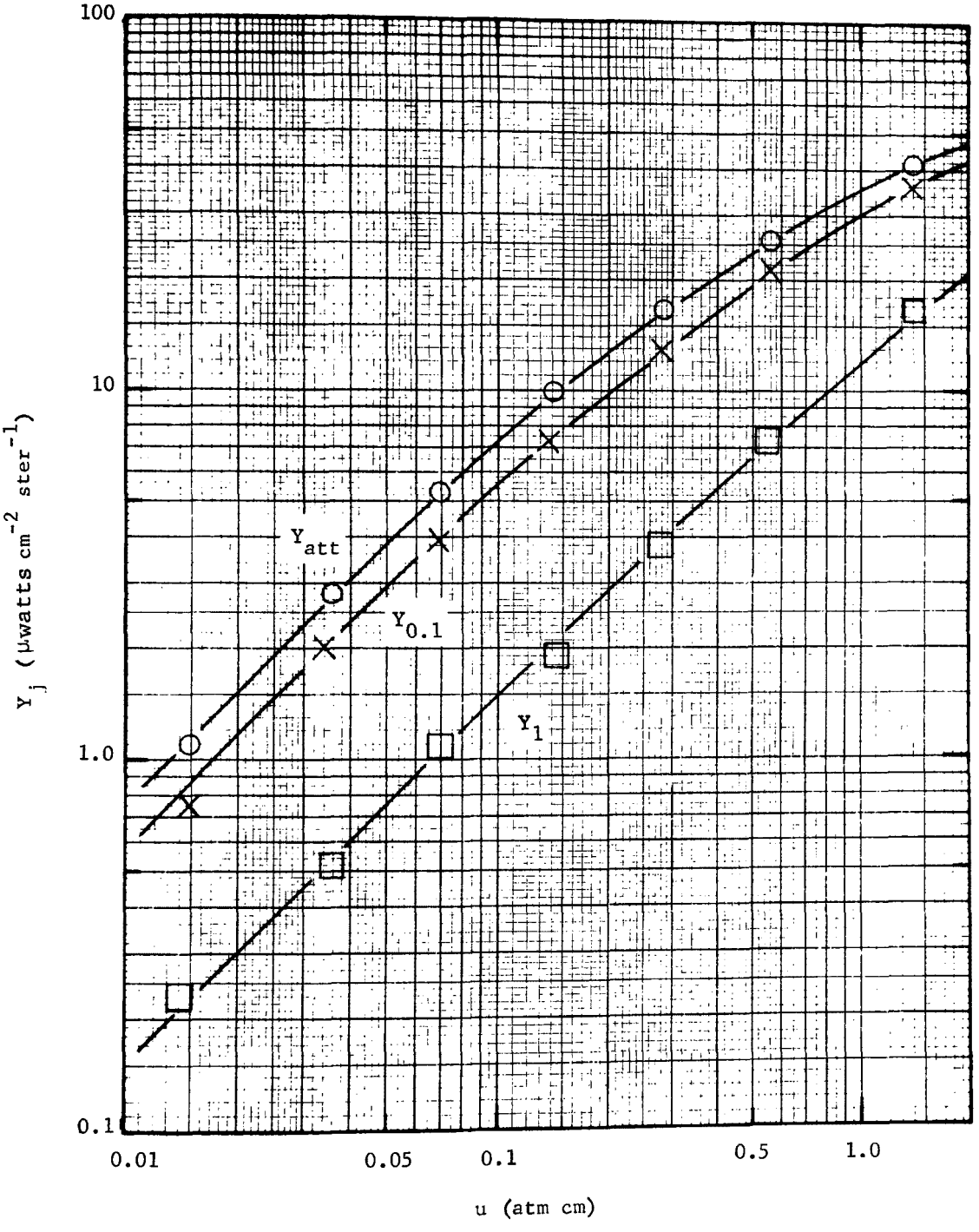

Figure 22. Logarithmic plots of Y_j vs u for NO + N_2 mixtures at 450 K. The continuum emission has been accounted for. Sample cell length, 1.42 cm.

Because of the correlation between the positions of the absorbing lines of the GFC and the emitting lines of the sample, the gas in the GFC is expected to absorb more of the energy from the hot gas than does the attenuator. However, the relatively small amount of gas in this GFC is opaque only over a very narrow spectral region near the center of each line. Therefore, this GFC does not absorb as much of the energy as the one that contains more NO. The absorption characteristics of these two GFC's correspond closely to the curves drawn in Figure 2 for the same values of w.

The measured values of Y_j may be in error by as much as 10 - 20% for the two smaller values of u (0.014 atm cm and 0.036 atm cm). This relatively large uncertainty is due to the small change in detector signal that results when one of these samples is added to the cell and to errors in correcting for the window emission. The percentage error is, of course, larger for the values of Y_1 than for the other two values of Y_{att} and $Y_{0.1}$ because the signal being measured is smaller. The percentage uncertainty in the values of Y_j decreases with increasing absorber thickness to approximately $\pm$ 5% for the sample of pure NO.

The concentrations of NO in the effluent of most stacks of interest are probably such that the u is between approximately 0.005 and 0.5 atm cm. If the stack diameter is 2.5 m, this would correspond to concentrations between 20 ppm and 2000 ppm of NO. These values of absorber thickness correspond to the lower portions of the curves of Figure 22 and to values lower than those plotted. For values of u lower than those plotted, Y_j can be assumed to be proportional to u. It is unlikely that many sources of interest will be large enough or contain enough NO to correspond to the larger values of u (between 0.5 and 2 atm cm) represented in Figure 22.

Most sources of NO produce plumes of the effluent that are more than 1 m in diameter. The 1.42-cm long sample cell used in this experiment can simulate sources for which the source dimension, ℓ, is much greater, but the concentration C is much less. To a good approximation, the emission of a sample at a given temperature and total pressure is a function of the product $C\ell$. Slight deviations from this can be expected to occur if the short cell contains samples with a NO concentration greater than approximately 30%. In this case, self-broadening of the NO emission lines causes their widths to be slightly different from those corresponding to a dilute mixture of NO in N_2 at the same total pressure.

Data similar to those represented in Figure 22 were also obtained for the same gas mixtures at three other temperatures; 431 K, 423 K and 406 K. Logarithmic plots of the data obtained at the other 3 temperatures have the same shapes as the corresponding curves in Figure 22. Of course, the values of Y_j for a given NO + N_2 mixture are lower for the lower temperatures, primarily because of the rapid decrease in the spectral radiance of a blackbody as the temperature decreases.

The values of Y_j for the different gas mixtures and different sample temperatures have been substituted into Equation (8) in order to determine the corresponding values of Z_1 and $Z_{0.1}$. These values have been plotted in Figure 23 for all four temperatures at which measurements were made. The values of Z_j are related to the amount of correlation between the spectral structures of the

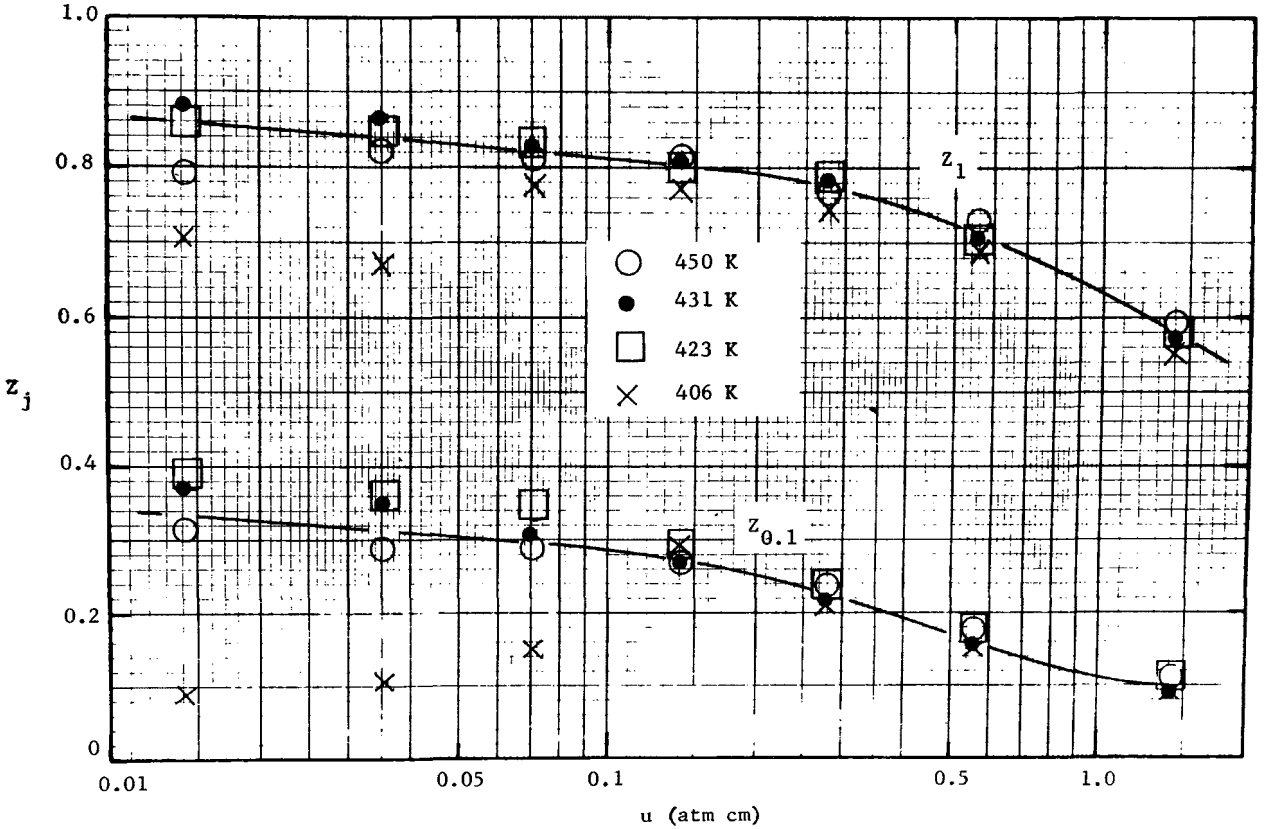

Figure 23. Semi-logarithmic plots of Z_j vs u for four sample temperatures. The continuum emission has been accounted for. The data points are based on measurements of Y_j similar to those represented by Figure 22.

emitting gas and the GFC. Z_j varies from 0 for an emitting sample that contains only continuum emission with no spectral structure, to a value of 1 for a case in which the GFC absorbs all of the energy emitted by the sample gas. By referring to the curves in Figure 2, we can see that Z_j is related to the fraction of the emitted energy that occurs within the narrow interval near each line center where the GFC absorbs strongly.

The data points in Figure 23 that represent 406 K samples with $u < 0.1$ atm cm fall well below the points corresponding to the same mixtures at higher temperatures. These unusually low values of Z_j are undoubtedly a result of some systematic error in measuring the corresponding Y_j's. There is no physical reason for Z_j to be lower for the smaller values of u than for larger values of u at the same temperature. As discussed above, the uncertainty in the measured values of Y_j is greatest for the small samples at the lowest temperatures.

A single curve represents, reasonably well, all of the data for a given GFC obtained at all four temperatures. This weak temperature dependence, along with a relatively weak dependence of Z_j on u, makes Z_j a convenient parameter to use along with measured values of Y_{att} to determine the NO concentration in an unknown sample. Low values of Z_j result when a large fraction of the emission is by continuum or by gases with spectral structure that has little or no correlation with the spectral structure of the gas species under study.

Although the data illustrated in Figure 23, with the exception of the erratic data corresponding to 406 K, show no apparent dependence on temperature, it is likely that a slight dependence could be observed if precise data were obtained over a wider temperature range. The shapes and strengths of spectral lines are known to change with increasing temperature; therefore, a slight dependence of Z_j on the temperature is probable.

The values of Z_j observed when using a hot NO source must be quite different from each other if the two measurements are to provide information about the absorption in different parts of the spectral line. The GFC with the most gas should absorb a large fraction of the energy emitted by a sample of hot gas only. For NO absorber thicknesses of most interest, Z_1 is greater than 0.75, indicating that 1 atm cm of NO is enough to make the GFC an efficient absorber of the energy emitted by the hot NO. Slightly larger values of Z_j could be obtained by using more NO in the GFC; however, this increase in efficiency would probably be more than offset by a loss in the discrimination against other gases.

The value of Z_j for GFC-c is strongly dependent on the emission within approximately 0.03 cm^{-1} of each line center and nearly independent of the emission outside of these very narrow spectral intervals. On the other hand, the value of Z_j for GFC-b, which contains more NO, is about equally sensitive to all of the emission any place within approximately 0.2 cm^{-1} of each line center. It follows that Z_j for GFC-c must be much less than Z_j for GFC-b when the emitting source is NO. This requirement seems to be satisfied; $Z_{0.1} \cong 0.3$ and $Z_1 \cong 0.8$ for values of u less than approximately 0.3 atm cm. If the amount of NO in GFC-c were reduced to less than 0.1 atm cm, Z_c would decrease and the sensitivity to emission for $(\nu - \nu_o) < 0.03$ cm^{-1} relative to that for $0.03 < (\nu - \nu_o) < 0.3$ cm^{-1} might increase slightly. This could slightly increase the amount of information provided by the two values of Z_j. However, a

practical lower limit on the amount of NO in GFC-c is that required to make the gas essentially opaque over an interval within about 0.02 - 0.03 cm^{-1} of the center of each strong NO line.

Although the amounts of NO in the two GFC's is not critical, the amounts used (1 atm cm and 0.1 atm cm) are probably about optimum for the spectral interval used. It is unlikely that the amount in GFC-c should be increased above the 0.1 atm cm being used; if any change is in order, the amount should probably be reduced. If the spectral interval were to be widened to include weaker NO absorption lines, a slight increase in the amount of gas in GFC-b could possibly improve performance, but it should not be increased significantly for the present spectral interval.

EMISSION BY SAMPLES CONTAINING NO + CONTINUUM EMISSION

The influence of adding continuum emission to the sample was observed by placing a 1 mm thick sapphire window adjacent to the 1.42-cm sample cell. The sapphire was placed in the beam on the side of the sample cell away from mirror M1 and was at essentially the same temperature as the sample cell. The sapphire was carefully placed with its surface perpendicular to the central portion of the beam of energy accepted by the instrument; therefore, there was no significant energy emitted by the hot furnace that was reflected from the surfaces of the sapphire window into the instrument. In the spectral interval of interest, the 1 mm thick sapphire at 450 K has an emissivity slightly greater than 0.06. The combination of this window and the windows of the sample cell produce an effective emissivity of 0.096.

The values of Y_j observed with this arrangement with different amounts of NO in the sample cell are plotted in Figure 24. These curves correspond to the curves of Figure 22, which represent samples of NO without any continuum emission. It is obvious that the values of Y_j should approach zero as u approaches zero when there is no continuum emission. However, as indicated by Figure 24, all of the values of Y_j approach a common constant level corresponding to the continuum emission as u becomes very small. When u = 0, $Y_{att} = Y_{0.1} = Y_1$ because of the method by which the alternator is balanced with no NO in the radiant energy source. All of the values of Y_j plotted in Figure 24 increase as u increases, and as in Figure 22, $Y_{att} > Y_{0.1} > Y_1$. As is to be expected, Y_1 increases very slowly for values of u less than approximately 0.1 atm cm. Most of the additional radiant energy emitted by the hot NO in the sample is absorbed by the GFC with 1 atm cm of NO.

Values of Z_j based on the data shown in Figure 24 have been plotted in Figure 25. The influence of continuum emission can be seen by comparing the curves of Figure 25 with the corresponding ones in Figure 23, which represent samples without continuum emission. It follows that Z_1 and $Z_{0.1}$ should approach zero as u becomes smaller.

The values of Z_1 plotted in Figure 25 reach a maximum of 0.5 at $u \cong 0.6$ atm cm. For larger values of u, Z_1 decreases as it does for increasing values of u when there is no continuum emission present. The maximum value of Z_1 is less than

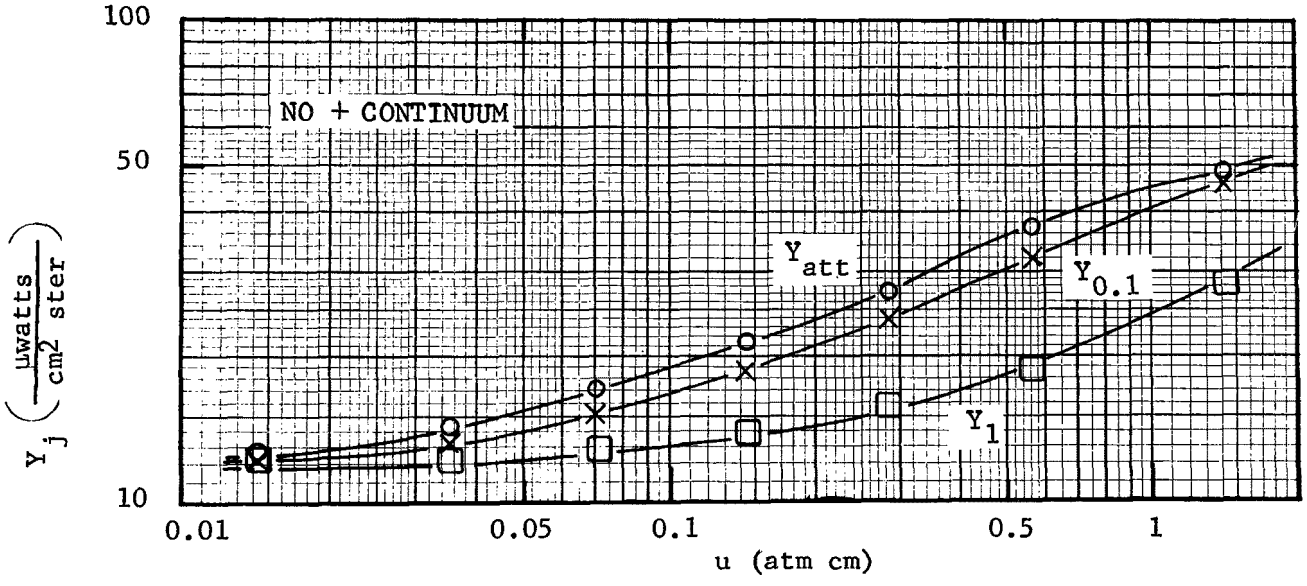

Figure 24. Logarithmic plots of Y_j vs u for samples of NO + N_2 with additional continuum emission. ϵ_c = 0.096. Sample temperature, 450 K. Sample cell length, 1.42 cm.

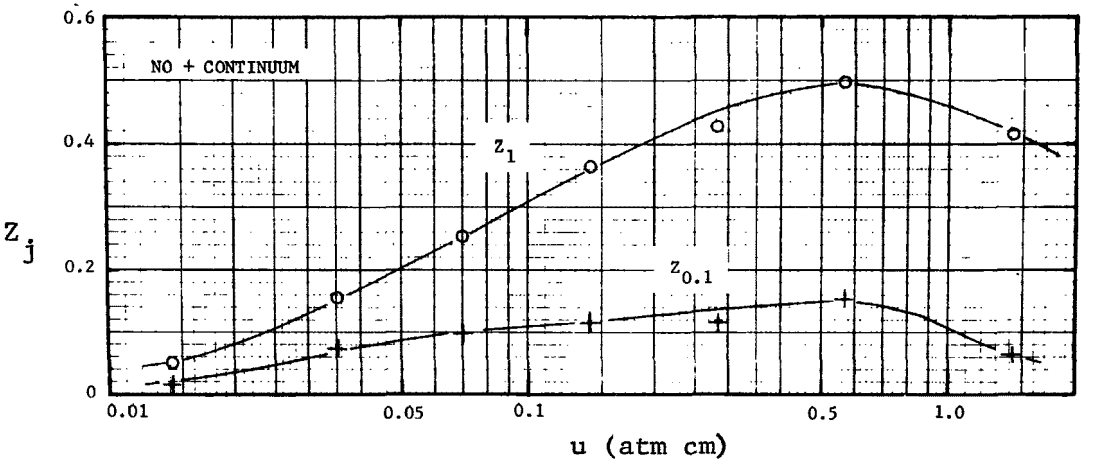

Figure 25. Semi-logarithmic plots of Z_j vs u for samples of NO + N_2 with additional continuum emission. The curves are based on the data shown in Figure 24.

the corresponding value of 0.73 for the same absorber thickness if no continuum is present. From the curves of Figure 21, we see that $\overline{\epsilon}_g \cong 0.22$ for u = 0.6 atm cm, the amount corresponding to the maximum value of Z_1 in Figure 25. As expected, the value of $Z_{0.1}$ increases more slowly than Z_1 as u increases. The estimated uncertainty in the values of Z_j is between 0.02 and 0.04. The shape of the curve corresponding to $Z_{0.1}$ cannot be determined accurately, but the decrease with increasing values of u greater than approximately 0.6 atm cm is significant.

Values of Y_j and Z_j corresponding to those in Figures 24 and 25 can be calculated for other values of continuum emissivity from the data presented in Figures 21, 22 and 23 for samples in which all of the emission is by NO. If the gas and the material producing the emission continuum are at the same temperature, ϵ (gas + continuum), the emissivity of the combination of gas and continuum, is related to ϵ_g, the emissivity of the gas only, and ϵ_c, the emissivity of the continuum only, by

$$\epsilon \text{ (gas + continuum)} = \epsilon_g + \epsilon_c - \epsilon_g \epsilon_c \quad . \tag{27}$$

It is assumed that ϵ_c is constant over the spectral interval of interest; it therefore follows that the corresponding values of Y_j are related by

$$Y_j \text{ (gas + continuum)} = (1 - \epsilon_c)\, Y_j \text{ (gas only)} + Y_j \text{ (continuum)}. \tag{28}$$

Values of $\underline{Y}_j$ (continuum) can be calculated for a known ϵ_c and sample temperature. Values of $\overline{\epsilon}_g$ can be obtained from the curves in Figure 21, making it possible to calculate Y_{att} (gas only). The values of Y_1 and $Y_{0.1}$ obtained from the curves of Figure 23 are valid for all temperatures between approximately 400 K and 450 K. These values make it possible to calculate Y_1 and $Y_{0.1}$ from the values of Y_{att} (gas only). Note that the only assumptions that have been made in the derivation of Equations (27) and (28) are: the emitting gas and continuum are at the same temperature; the spectral radiance of a blackbody is constant over the entire spectral interval; and the emissivity of the continuum is assumed to be constant over the entire spectral interval. Because of the narrow spectral interval used, these assumptions can be made without introducing significant error to the data. The experimental values of Y_j and Z_j shown in Figures 24 and 25 agree within the expected uncertainty with calculated values based on the known continuum emissivity (ϵ_c = 0.096) and the data for NO emission given in Figures 21, 22 and 23.

H_2O INTERFERENCE

Because of the potentially troublesome interference by H_2O in the remote sensing of NO, we have performed a series of measurements on the absorption and emission by H_2O samples that are representative of the H_2O in the effluent from a stack. The samples were contained in the 200-cm sample cell illustrated in Figure 19. All of the samples were at 445 K and consisted of either pure H_2O or of $H_2O + N_2$ at a total pressure of 1 atm. The results are summarized in Table 3.

TABLE 3

SUMMARY OF H_2O INTERFERENCE DATA

Interval	1896.0-1907.0 cm^{-1}			1888.5-1899.5 cm^{-1}		1900.5-1911.5 cm^{-1}	
% H_2O	1.4% (Air)	30%	100%	10%	30%	10%	30%
$\frac{\overline{T_s T_{att}}}{\overline{T_{att}}} = \overline{T}_s$	0.983	0.672	0.152	0.774	0.461	0.826	0.557
$\frac{\overline{T_s T_1}}{\overline{T_1}}$	0.984	0.639	0.136	0.764	0.459	0.799	0.506
$\frac{\overline{T_s T_{0.1}}}{\overline{T_{0.1}}}$	0.981	0.672	0.148	0.773	0.462	0.826	0.547
Y_{att} (a)	3.06	59.04	156	40.7	97.0	31.3	79.7
Y_1	3.36	63.7	158	41.2	100.6	35.5	88.0
$Y_{0.1}$	3.02	58.4	155	39.1	96.5	31.3	79.0
Z_1 (transmission) (b)		-0.101	-0.019	-0.044	-0.037	-0.155	-0.115
$Z_{0.1}$ (transmission)		0	-0.005	-0.004	-0.002	0	-0.023
Z_1 (emission) (b)	-0.098	-0.079	-0.013	-0.012	-0.037	-0.133	-0.104
$Z_{0.1}$ (emission)	0.013	0.011	0.006	0.039	0.005	0.001	0.009

(a) Values of Y are in μwatts cm^{-2} $ster^{-1}$.

(b) Values of Z are based on the transmission data or emission data, as indicated.

Three spectral intervals were employed, corresponding to curves A, B, and C in Panel III of Figure 20. The 1896.0 - 1907.0 cm^{-1} interval is represented by curve B and is the one used to obtain the NO data presented previously. A few data on H_2O interference were obtained in the other two intervals to determine the influence of relatively strong H_2O absorption lines that occur just outside of the 1896.0 - 1907.0 cm^{-1} interval. The first column of data listed in Table 3 correspond to a sample of 1 atm of air let into the sample cell. The H_2O content was not measured, but it was probably near 1.4%. Each of the other columns represents samples of either H_2O or $H_2O + N_2$ with the H_2O concentrations indicated.

The first line of Table 3 gives the average transmittances of the samples as they were measured with the monitoring beam passing through the attenuator. Because T_{att} is constant over the spectral interval passed by the instrument, this quantity represents the average transmittance of the sample. All of the tabulated values of transmittance are somewhat greater than they would be if the approximately 9-meter optical path through the air were free of H_2O. The air contained approximately 1.4% H_2O and absorbed some of the energy near the H_2O absorption lines. Although the atmospheric H_2O absorbed when the H_2O sample was in the cell as well as when the cell was empty, the atmospheric H_2O still increases the average transmittance that is measured. The primary purpose of these measurements was to provide data from which the potential interference of H_2O in a field instrument can be estimated. Elimination of the H_2O in the atmospheric path would probably not significantly change the estimated interference. Furthermore, a field instrument will be required to operate through much longer atmospheric paths, so that the effort required to eliminate the H_2O from the optical path during the laboratory measurements was not justified.

The quantities tabulated in lines 2 and 3 of Table 3 were obtained in the same manner as the values in line 1, except that the attenuator was replaced in the monitoring beam by either of the two GFC's. The method of obtaining the data and the definitions of the terms are given at the end of Section VI. The relative values of the three transmittance ratios listed in lines 1, 2 and 3 for a given sample are probably accurate to approximately $\pm$ 0.002. Uncertainties in the content of the mixtures may cause the transmittance ratios to be in error by as much as 0.02. This relatively large uncertainty is unimportant for the present purposes because the potential interference by H_2O depends mostly on the differences between the transmittance ratios tabulated.

The H_2O absorber thickness of the 30% samples is 60 atm cm, the amount of H_2O in a 6-meter diameter stack with 10% H_2O. This is probably typical of some of the larger stacks of interest, although some stacks may be even larger. The H_2O absorber thickness (20 atm cm) of the 10% samples is probably more representative of the average stacks to be investigated. Note that the average transmittance of the 100% sample is only approximately 0.15. This corresponds to an average emissivity of 0.85, which is sufficiently high to make it difficult to measure the emission by NO, even if there were no interference caused by correlation between the spectral structures of the H_2O and the NO.

It is well known that the collision half-widths of H_2O absorption lines for a sample at 1 atm total pressure are much greater when the sample consists of pure

H_2O than when the sample consists of H_2O in a dilute mixture with N_2. Collisions of the absorbing H_2O molecules with other H_2O molecules are more effective in broadening the lines than are collisions of the absorbing H_2O molecules with N_2. Because of this, the lines corresponding to 100% H_2O sample are probably about five times as wide as if the sample were a dilute mixture of H_2O in N_2. Thus, the results tabulated for the 100% sample cannot be applied directly to a stack for which the H_2O absorber thickness is the same, 200 atm cm. The average transmittance of a dilute mixture of 200 atm cm of H_2O in N_2 would probably be between 0.25 and 0.30. Self-broadening of the H_2O lines also has an effect on the 30% mixture, but the effect is much less because of the lower H_2O concentration.

The procedure discussed at the end of Section VI has been applied to the transmittance ratios listed in Table 3 to calculate the values of Z_1 and $Z_{0.1}$ that appear in the 7th and 8th lines of the table. No values of Z are given for the 1.4% H_2O mixture because its absorption is so low that the small difference between the measured transmittance ratios is no more than the experimental uncertainty. All of the values of Z_1 are seen to be negative, which indicates that there is a slight negative correlation between the positions of the H_2O lines and the NO lines in the spectral interval passed by the grating assembly.

A review of Figure 2 can be helpful in understanding the basis for this negative correlation. Consider curve D of the figure, which closely resembles a plot of the transmittance of a single NO line for the GFC that contains 1 atm cm of NO. An H_2O line would contribute to positive interference and have a positive correlation with the NO if the H_2O line occurred where curve D of Figure 2 lies below the average transmittance of the attenuator, which for the example in Figure 2 is 0.7415. On the other hand, if the H_2O line occurs more than approximately 0.45 cm^{-1} from the center of the NO line, it will produce a negative correlation because the gas in the GFC transmits more than the attenuator in this spectral interval. The usually good discrimination of a GFC instrument depends on a near-random relationship between the positions of the absorption lines of the gas to be measured and the lines of other gases to be discriminated against. If the lines of the interfering gas are spaced so that those that produce a negative correlation exactly cancel those that produce a positive correlation, there will be no interference in the measurement as long as the average attenuation of the potentially interfering gas is accounted for. If the absorption by another gas produces constant attenuation across the spectral interval, it will behave as a continuum absorption or emission and will not contribute to Z.

Because of the consistent negative values of Z_1, we conclude that the strongest H_2O emission lines occur sufficiently far from the strong NO lines that they produce enough negative interference to more than offset the contribution by the lines that produce positive interference. The amount of correlation is obviously dependent on the spectral bandpass and is difficult to calculate accurately on the basis of known parameters of the NO and H_2O lines. However, the negative correlation could probably be predicted from a careful examination of spectra of H_2O and NO such as those shown in Figure 20. None of the prominent H_2O lines occur within a few tenths of a cm^{-1} of the centers of the strong NO lines.

Because of the very narrow interval near each line center over which there is strong absorption by the GFC containing 0.1 atm cm, the value of $Z_{0.1}$ is much

smaller than that observed with the other GFC. The values of $Z_{0.1}$ based on the transmission measurements are also negative; however, their magnitude is approximately equal to the uncertainty in the measurements.

Comparison of the values of $\bar{T}_s$ of the 30% H_2O mixtures for the three different spectral intervals illustrates the importance of choosing the proper spectral interval. The 1896.0 - 1907.0 cm^{-1} interval was chosen to minimize H_2O absorption and emission. The increased average absorptance in the other two intervals, represented by curves A and C in Panel III of Figure 20, is predictable from the H_2O spectra of Figure 20. It is interesting to note that although the H_2O absorption is greater in these two "shifted" spectral intervals, the absolute value of Z_1 for the 30% mixtures is not increased appreciably. In fact, the absolute value of Z_1 based on the transmission data for the 30% sample in the 1888.5 - 1899.5 cm^{-1} interval is less than the corresponding value for the higher wavenumber interval with less average absorption.

The values of Y_{att}, Y_1 and $Y_{0.1}$ for H_2O listed in lines 4, 5 and 6 of Table 3 were obtained by measuring the emitted energy by the same method used for the NO. The continuum emission, by mirror MC and the windows of the 2-meter cell, was accounted for by the same procedure used to account for the continuum emission by the windows of the 1.42 cm cell. The combined emissivity of mirror MC and the 2 windows was approximately 0.08. The values of Z_1 based on the emission data are in fair agreement with the corresponding values based on the transmission data. The main contributors to the differences in the two values are probably errors in accounting for the continuum emission and to instabilities in the optical components, including variations in the amount of H_2O in the atmospheric path through which the radiant energy beam passed. Some of the difference may be due to the extra length (approximately 1 m) of the atmospheric path through which the radiant energy passes for the transmission measurement.

The absolute values of $Z_{0.1}$ based on the emission data are in most cases too small to be significant. The relatively large value of 0.039 for the 10% mixture with the 1888.5 - 1899.5 cm^{-1} interval is the only value that is significantly greater than the estimated uncertainty. There is no apparent explanation for this unusually high value.

The interference by H_2O can be discussed more easily if we treat the H_2O emission as if it consisted of two separate parts, the non-correlated part and the correlated part. The non-correlated part can be treated as if it were continuum emission. This non-correlated portion of the emitted energy would contribute exactly the same amount to the values of Y_{att}, Y_1 and $Y_{0.1}$; thus Z_1 and $Z_{0.1}$ would equal zero. It is not necessary that the non-correlated portion be constant over the entire spectral interval in order for Z_1 and $Z_{0.1}$ to be zero. It is only necessary that there be no correlation, either positive or negative, between the spectral structures of this portion of the emitted energy and the absorption by the GFC's. The correlated portion can be thought of as the energy emitted by a given amount of NO. If this correlated portion contributes to positive values of Z_1 and $Z_{0.1}$, it is equivalent to a positive amount of NO.

Consider the results obtained in emission in the 1896.0 - 1907.0 cm^{-1} region (Table 3) for the 60 atm cm of H_2O sample that consists of 30% H_2O + 70% N_2.

Note that $Z_1 = -0.079$; the negative value indicates that the correlated portion corresponds to a negative amount of NO. As is seen in Table 3, it is possible for Z_1 to be negative while $Z_{0.1}$ is positive; it would also be possible for the signs to be reversed for a different interfering gas. Because of the difference in the signs (+ or -) of Z_1 and $Z_{0.1}$, it is apparent that what has been defined as the non-correlated part of the emission depends on which GFC is being used. Thus, the concept of interfering emission being composed of a correlated part plus a non-correlated part is limited in its value and can not be dealt with in a simple algebraic manner. Nevertheless, the concept is useful in discussing the different ways in which the H_2O emission interferes with NO measurements and how it can be accounted for.

It is apparent from the data in Table 3 that hot H_2O in the stack effluent being monitored for NO can produce serious interference. Let us assume for the sake of discussion that $Z_1 = Z_{0.1} = 0$ for the 30% H_2O mixture. This is equivalent to assuming that all of the H_2O emission is non-correlated and would minimize the interference problem to that of dealing with continuum emission for which $\epsilon_c = (1 - \overline{T}_{H_2O}) = (1 - 0.672) = 0.328$. Even with this simplified problem, it is difficult to estimate the accuracy to which the concentration of NO could be measured in a stack containing this much H_2O. The value of $Z_{0.1}$, which is proportional to the difference between Y_{att} and $Y_{0.1}$, is very small and must be measured quite accurately when ϵ_c is this large. The value of Z_1 is larger than $Z_{0.1}$, and can be measured somewhat more accurately. When the effluent temperature is unknown, both Z_1 and $Z_{0.1}$ must be measured accurately in order to determine the NO concentration. If the temperature could be determined by some other method, an accurate measurement of $Z_{0.1}$ would not be required, and the NO concentration could be determined from measurements of Y_{att} and Y_1. It is unlikely that a field instrument would be capable of measuring Z_1 with an uncertainty of less than 0.01 under the best conditions. This would correspond to $\overline{\epsilon}_{NO} \cong 0.004$ when $\overline{\epsilon}_{H_2O} = 0.328$. By extrapolating the 450 K curve of Figure 21, we see that this corresponds to a minimum detectable NO absorber thickness u of approximately 0.005 atm cm (50 ppm - m), which would be quite adequate for many applications.

If the gas temperature is not known, as is usually the case, the minimum detectable u would probably increase by at least a factor of 4 to 10 because of the reliance on an accurate measurement of $Z_{0.1}$. This minimum detectable u, 0.02 - 0.05 atm cm, is probably too large for most applications. Of course, the effluent of many stacks contains much less H_2O than is used in this example; as the amount of H_2O decreases, the minimum detectable u for NO will also decrease accordingly.

The correlated part of the interfering H_2O emission further complicates the reduction of the data and adds to the errors. If, for example, emission from the 30% mixture were treated as if all of the H_2O emission were non-correlated, the $Z_1 = -0.079$ would lead to an NO absorber thickness of approximately -0.02 atm cm. A negative absorber thickness has no physical meaning, but if NO were also present in the emitting sample, the measured NO absorber thickness would be too low by 0.02 atm cm. Many gas-filter correlation instruments of various types are troubled by interference from gas species other than the one being measured. By previously measuring the amount of interference by known quantities of the

interfering gas, it is possible to account for the interfering gas and reduce the error caused by it. This method can also be used, but to a lesser degree, on a field instrument of the type considered here. The H_2O interference could be measured for a variety of H_2O samples of known concentration; the data could then be used along with estimates of the amount of H_2O in the stack to calculate the interference. This procedure is much more complex for this type of field instrument than for a laboratory instrument that operates under stable conditions with a known sample temperature. It is almost certain that the amount of interference by a known amount of H_2O depends on its temperature, which is usually unknown.

Absorption by the H_2O in the atmospheric path also complicates the interference problem. Much of the error due to H_2O absorption can be accounted for by balancing the three components (attenuator, GFC-b and GFC-c) of the alternator while using a continuous emitter located near the stack as the energy source. The hot surface of the stack just below the top might serve for this purpose. By balancing the alternator in this manner, the correlated portion of the H_2O absorption will not produce errors as it would if the atmospheric paths were quite different when measurements were made than when the alternator was balanced. Possible errors due to the atmospheric H_2O absorption are not completely eliminated in this manner because of the strong correlation between the spectra of the emitting H_2O and the absorbing H_2O. The absorbing H_2O changes the spectral characteristics of the energy emitted by the hot H_2O that reaches the instrument. Thus, the correction that would have to be made for interference by emitting H_2O depends on the amount of H_2O in the absorbing path as well as on the temperature and amount of hot H_2O in the emitting gas.

Still another mechanism for possible H_2O interference exists because of emission by atmospheric H_2O. The amount of radiant energy involved in this process is low because of the low spectral radiance of a blackbody at typical atmospheric temperatures. The H_2O involved in this process includes not only that between the hot gas source and the instrument, but also the atmospheric H_2O in the line-of-sight beyond the hot gas source. Particularly on a cloud-free day, the energy emitted by the distant atmosphere has emission maxima due to H_2O emission. The correlated part of the structure in this background emission could also produce small errors if it is not accounted for. Fortunately, the interference by this background emission can probably be measured by pointing the receiver off to the side of the stack gas so it is observing an atmospheric path very similar to the one in the field-of-view during the measurements.

A carefully designed GFC field instrument of the type considered here with a present day state-of-the-art interference filter and a liquid-nitrogen-cooled detector would probably be limited in its accuracy by H_2O interference. The minimum detectable thickness of NO for stacks of interest would probably vary from less than 0.005 atm cm to more than 0.1 atm cm. The minimum value corresponds to a stack with little H_2O in its effluent if the temperature can be determined by another independent method. The larger value corresponds to larger stacks with more H_2O and with no a-priori knowledge of the temperature. These estimates are based on an atmospheric path between approximately 100 m and 200 m and on the assumption that the H_2O content of the effluent can be estimated by other methods. It is also assumed that the continuum emissivity due to particulate matter is less than about 0.1 and that no effluent gases other than H_2O produce any significant interference.

REFERENCES

1. Burch, D. E. and D. A. Gryvnak. Infrared Gas Filter Correlation Instrument for In-Situ Measurement of Gaseous Pollutants. EPA-650/2-74-094, Environmental Protection Agency, Washington, D.C, Prepared by Aeronutronic Ford Corp., under Contract No. 68-02-0575, December 1974. Also, Burch, D. E. and D. A. Gryvnak, "Cross-Stack Measurement of Pollutant Concentrations Using Gas-Cell Correlation Spectroscopy", Chapter 10 of Analytical Methods Applied to Air Pollution Measurements, R. K. Stevens and W. F. Herget (Eds.) Ann Arbor Science Publishers, Ann Arbor, Michigan, 1974, pp 193-231.

2. Shaw, J. H. Nitric Oxide Fundamental. J. Chem. Phys. 24:399-402, 1956.

3. Abels, L. L. and J. H. Shaw. Width and Strengths of Vibration-Rotation Lines in the Fundamental Band of Nitric Oxide. Journ. Molecular Spectroscopy 20:11-28, 1966.

4. Gryvnak, D. A. and D. E. Burch. Monitoring NO and CO in Aircraft Jet Exhaust by a Gas-Filter Correlation Technique. AFAPL-TR-75-101, Air Force Wright Aeronautical Laboratories, Wright-Patterson Air Force Base, Ohio. Prepared by Aeronutronic Ford Corp., under Contract No. F33615-75-C-2038, Jan. 1976.

TECHNICAL REPORT DATA
(Please read Instructions on the reverse before completing)

1. REPORT NO.	2.	3. RECIPIENT'S ACCESSION NO.
EPA-600/2-76-277		

4. TITLE AND SUBTITLE	5. REPORT DATE
REMOTE MONITORING OF NITRIC OXIDE BY GAS-FILTER CORRELATION TECHNIQUES	November 1976
	6. PERFORMING ORGANIZATION CODE

7. AUTHOR(S)	8. PERFORMING ORGANIZATION REPORT NO.
Darrell E. Burch and David A. Gryvnak	U-6252

9. PERFORMING ORGANIZATION NAME AND ADDRESS	10. PROGRAM ELEMENT NO.
Aeronutronic Ford Corporation Aeronutronic Division Ford Road Newport Beach, California 92663	1AD712 (1AA010)
	11. CONTRACT/GRANT NO.
	68-02-0766

12. SPONSORING AGENCY NAME AND ADDRESS	13. TYPE OF REPORT AND PERIOD COVERED
Environmental Sciences Research Laboratory Office of Research and Development U. S. Environmental Protection Agency Research Triangle Park, N.C. 27711	Final, 6/73-6/76
	14. SPONSORING AGENCY CODE
	EPA-ORD

15. SUPPLEMENTARY NOTES

16. ABSTRACT

The feasibility of remotely monitoring the concentration of Nitric Oxide (NO) in the effluent of industrial stacks has been investigated analytically and experimentally in the laboratory. The type of instrument considered employs two or more gas-filter cells that contain different amounts of NO. Radiant energy emitted by the hot gas in the effluent is measured after it has passed either through one of the gas-filter cells or through a neutral density filter. By comparing the amounts of energy received through each of the filters, it is possible to determine the concentration of NO in the presence of a moderate amount of continuum-emitting material such as small particles. A simple, single-line spectral model served as the basis for the analytical work. Heated cells containing NO + N_2 or H_2O + N_2 simulated an industrial stack for the laboratory experiments. Interference by hot H_2O in the effluent and cold H_2O in the atmospheric path causes the most serious uncertainties in the measurements for many types of stacks.

17. KEY WORDS AND DOCUMENT ANALYSIS

a. DESCRIPTORS	b. IDENTIFIERS/OPEN ENDED TERMS	c. COSATI Field/Group
*Air Pollution *Nitric Oxide *Remote Sensing Monitors	Gas-Filter Correlation	13B 07B 14B

18. DISTRIBUTION STATEMENT	19. SECURITY CLASS *(This Report)*	21. NO. OF PAGES
RELEASE TO PUBLIC	UNCLASSIFIED	80
	20. SECURITY CLASS *(This page)*	22. PRICE
	UNCLASSIFIED	

EPA Form 2220-1 (9-73)